N88-22492

A Multivariate Variational Objective Analysis - Assimilation Method, Part II: Case Study Results with and without Satellite Data.

Gary L. Achtemeier, Stanley Q. Kidder, and Robert W. Scott

Climate and Meteorology Section
Illinois State Water Survey
Champaign, IL 61820

A Multivariate Variational Objective Analysis - Assimilation Method, Part II: Case Study Results with and without Satellite Data.

Gary L. Achtemeier, Stanley Q. Kidder,

and Robert W. Scott

Climate and Meteorology Section

Illinois State Water Survey

Champaign, IL 61820

ABSTRACT

The variational multivariate assimilation method described in a companion paper by Achtemeier and Ochs is applied to conventional and conventional plus satellite data. Ground-based and space-based meteorological data are weighted according to the respective "measurement" errors and blended into a data set that is a solution of numerical forms of the two nonlinear horizontal momentum equations, the hydrostatic equation, and an integrated continuity equation for a dry atmosphere. The analyses serve first, to evaluate the accuracy of the model, and second, to contrast the analyses with and without satellite data. Evaluation criteria measure the extent to which a) the assimilated fields satisfy the dynamical constraints, b) the assimilated fields depart from the observations, and c) the assimilated fields are judged to be realistic through

pattern analysis. The last criterion requires that the signs, magnitudes, and patterns of the hypersensitive vertical velocity and local tendencies of the horizontal velocity components be physically consistent with respect to the larger scale weather systems.

The method was applied to the 0000 GMT 11 April 1979 (SESAME I) dataset. Results show that the blended data sets converge to the solution of the four dynamical constraints by 90-100 percent. The pattern analysis shows that the variational analysis was able to retain major synoptic and regional scale meteorological features in conventional and hypersensitive variables. The variational analysis accurately diagnosed fields of the tendencies of the horizontal velocity components. These tendencies were combined with the adjusted velocity components at the synoptic time to predict the wind field at 0300 GMT. Comparisons between the predicted and observed wind fields are very encouraging given that the wind field was disturbed by a major mesoscale convective system.

1. Introduction

In a companion paper, Achtemeier and Ochs (1988) describe a multivariate data assimilation model based upon the variational method of undetermined Lagrange multipliers (Sasaki, 1958, 1970). It is the first of several variational numerical models of increasing complexity designed to produce fields of meteorological variables that are solutions of difference approximations of the Navier-Stokes equations. The variational model (MODEL I) evaluated in this article includes dynamical constraints: the two nonlinear horizontal momentum equations, the hydrostatic equation, and an integrated

continuity equation for a dry atmosphere. Later versions will include the thermodynamic equation, moist processes, and the radiative transfer equation.

The method incorporates data from diverse sources and with different measurement accuracies, and, in particular, it meshes observations from space-based platforms with those from more traditional immersion techniques. However, there are some quantities which, because of poor instrument accuracy or insufficient sampling frequency, cannot be measured directly and must be inferred through functions of other measured variables. These evolve as part of the variational blending processes and include hypersensitive variables such as vertical velocity and the local tendencies of the horizontal velocity components that are sensitive to small changes in the other variables. The velocity component tendencies are explicit in the dynamic constraints and therefore must be solved for in the variational formulation. A discussion of other methods for diagnosing local tendencies is found in the companion paper.

The purposes of this paper are (1) to demonstrate that the variational assimilation performs as predicted by theory and (2) to compare multivariate variational objective analyses with and without satellite data. Because this assimilation is not an initialization for a numerical prediction model, identifying the best analysis as that which produces the best forecast does not apply. Alternatively, three diagnostic criteria are used, which, although they may be somewhat more subjective than measures of forecast skill, have found use in the verification of diagnostic analyses (Krishnamurti, 1968; Achtemeier, 1975; Otto-Bliesner et al., 1977). These criteria are measures of a) the extent to which the assimilated fields satisfy the dynamical constraints, b) the extent to which the assimilated fields depart from the

observations, and c) the extent to which the assimilated fields are realistic as determined by pattern analysis. The last criterion requires that the signs, magnitudes, and patterns of the vertical velocity and local tendencies of the horizontal velocity components be physically consistent with respect to the larger scale weather systems.

The methods used to prepare the data for insertion into MODEL I are described in the Section 2. Section 3 develops the precision moduli that weight the data in the assimilation. The evaluation of MODEL I and comparisons of assimilations with and without satellite data are presented in Section 4. The results of this study are discussed in Section 5.

2. Preparation of Data for the Variational Analysis

The NASA AVE/SESAME I data set was used to evaluate MODEL I. An intense jet streak rounding a major trough located over the western United States (Fig. 1) produced an outbreak of severe convection over the plains of Texas and Oklahoma near 0000 GMT 11 April 1979. This case was selected because TIROS-N temperature soundings coexisted with special 3-hr rawinsonde data over a large area of the central United States during a major cyclogenesis. The 3-hr rawinsonde data were used to to verify diagnosed 3-hr local tendencies of the horizontal velocity components. Furthermore, this case has been the subject of several synoptic and mesoscale analyses. Results from some of these studies are useful for the evaluation of MODEL I.

One disadvantage of this data set is that intense mesoscale convective systems significantly impacted the large scale dynamics. These systems are

evident in the major cloud pattern over Oklahoma (Fig. 2). Resolution of mesoscale systems was not part of the design for this study. We attempted to minimize, but not eliminate, the impacts of these systems by using only rawinsonde data from the NWS synoptic network for the evaluation. Fig. 3 distributs rawinsonde and TIROS-N temperature soundings. The analysis grid is enclosed by the large, solid rectangle. The evaluation grid is enclosed by the large dashed rectangle. The SESAME I network used for evaluation of the diagnosed velocity component tendencies is shown by the smaller dashed rectangle.

The ten level model has the state variables staggered in both the horizontal and vertical dimensions. The grid template (see Fig. 4) is the so-called Arakawa D-grid. Mesinger and Arakawa (1976) have shown that phase speed and dispersion properties of this staggered grid make it inferior relative to other grid configurations for numerical prediction. However, the D-grid is well suited for the variational equations. The variables u, v, Φ, and the developmental components, ε_u and ε_v, (Achtemeier and Ochs, 1988) are located on primary coordinate surfaces at approximate 100 mb intervals from the top of the domain (100 mb) to the surface. T and σ appear at the half-levels. The upper boundary on σ is at 50 mb (σ=0) and the lower boundary (σ=0) is the ground. In the configuration of variables, the average conditions of the lowest sigma layer are represented by the surface observations. Therefore, the mean divergence of this lowest layer is represented by the boundary layer divergence.

The nonlinear vertical coordinate blends terrain-following coordinates in the lower troposphere with pressure coordinates in the middle and upper

troposphere. It is designed so that the coordinate surfaces are standard pressure levels above a reference pressure level, p^*. This allows direct incorporation of TIROS-N mean layer temperatures (data bounded by pressure surfaces) directly at these levels without any need for complex vertical interpolation that would arise with "standard" sigma coordinates where terrain effects extend to 100 mb. The method also eliminates the need for vertical interpolation at the end of the variational analysis in order to interpret the final analyses.

The procedure to place model variables on the sigma levels requires that all variables, except for the surface winds and temperatures, be initially gridded to constant pressure surfaces. The surface winds and temperatures which are gridded directly to the lower coordinate surface. The Achtemeier (1987) modification of the Barnes (1964) successive corrections technique interpolates observations onto the 40 by 25 analysis mesh with 100 km grid spacing (Fig. 3). Analysis errors in first and second derivatives calculated from fields of interpolated data are decreased by this method (Achtemeier, 1988). This is an important consideration for an assimilation method that contains many mathematical terms having derivatives and derivative products.

Sigma coordinate surfaces are pressure surfaces at heights at and above the reference pressure level. Sigma surfaces below p^* were calculated to maintain hydrostatic balance between temperature, pressure and height. We nondimensionalized all variables and, following the theory developed in the companion paper, removed most of the terrain-caused vertical variations of pressure and height through a transformation onto equivalent pressure surfaces. Finally, we removed a hydrostatic reference atmosphere and carried

out the variational adjustments on the residual variables.

Biases in satellite soundings have been the subject of a number of investigations (Phillips et al., Schlatter, 1981; Gruber and Watkins, 1982). A bias study by Kidder and Achtemeier (1986) revealed no significant elevation bias but did reveal a day-night bias. These biases were removed prior to insertion into the model.

Since satellite soundings are not made simultaneously with the semi-daily balloon soundings from the National Weather Service upper air network, we considered several simple time-to-space conversions to make the satellite soundings more representative at synoptic times. Very small correlations were found when the calculated changes were compared with the actual temperature changes measured by rawinsonde at 3-hr intervals over the NASA AVE/SESAME network for 10-11 April 1979. Therefore, the satellite data were blended directly into the analysis.

3. Precision Modulus Weights for the Variational Assimilation

The gridded fields of meteorological variables to be assimilated by the variational method are meshed with the dynamic constraints through the formulation described in the companion paper. We emphasize however, that the fields to be adjusted are obtained through univariate objective interpolation. (Another approach would blend the variational formalism with an optimized successive corrections method similar to that proposed by Bratseth (1986).) Therefore, the relative weights accorded to the gridded fields should be

functions of both observation and interpolation errors. We neglect the interpolation errors for the following reasons. First, this analysis is done for a data-rich area for which interpolation error should be relatively small. Second, observation errors for a single case should depart somewhat from "standard" observation errors which are calculated from a large ensemble of cases. Third, several meteorological variables are not observed directly. The precision moduli for these variables must be calculated from functional relationships with those that are observed. Heuristically, uncertainties introduced by our inability to accurately estimate the observational error should at least equal and probably exceed the interpolation error.

The gridded variables receive precision modulus weights in proportion to their relative analysis accuracies according to

$$\pi_i = \pi^*_i(\sigma)G_i(x,y) \qquad (1)$$

where π^* for the ith variable is defined by $\pi^*_i = (2\sigma_i^2)^{-1}$ (Whittaker and Robinson (1926). The σ_i is the root mean square (RMS error for the ith variable. G_i is in general a function of observation density but $G_i \equiv 1$ for this study.

The Lagrangian density (Eqn. 40 in the companion paper),

$$\begin{aligned} I = {} & \pi_1 (u-u^o)^2 + \pi_1 (v-v^o)^2 + \pi_2 (\dot{\sigma}-\dot{\sigma}^o)^2 + \pi_3 (\phi-\phi^o)^2 \\ & + \pi_4 (\overline{T}-\overline{T}^o)^2 + \pi_5 (\phi_x - \phi_x{}^o)^2 + \pi_5 (\phi_y - \phi_y{}^o)^2 + \pi_6 (\phi_\sigma - \phi_\sigma{}^o)^2 \\ & + \pi_7 (\xi_u - \xi_u{}^o)^2 + \pi_7 (\xi_v - \xi_v{}^o)^2 + 2\lambda_1 M_1 + 2 \lambda_2 M_2 + 2 \lambda_3 M_3 \\ & + 2 \lambda_4 M_4 \end{aligned} \qquad (2)$$

contains precision modulus weights for the adjustable variables and their derivatives. The precision moduli, π_1, π_3, and π_4, weight the observed horizontal wind components, geopotential height, and the layer mean temperature. Further, π_5 and π_6 weight gradients of observed geopotential and the remaining precision moduli π_2 and π_7 weight the vertical velocity and the developmental components of the local velocity component tendencies.

Standard observation errors available in the meteorological literature are used to calculate precision moduli for observed variables. Other precision moduli must be calculated from these standard errors. If the measurement errors are uncorrelated and if the representative gradient is the average separation between observing sites, then the RMS error for the geopotential gradient is related to the RMS error for the geopotential by

$$\sigma_{\phi_x} = \sigma_{\phi_y} = \frac{\sqrt{2}\,\sigma_\phi}{\Delta S} \tag{3}$$

where S is the average separation between observation sites. The error in the geopotential thickness is related to the measurement error in the mean temperature for the layer through the hydrostatic equation. In sigma coordinates it is

$$\sigma_{\phi_\sigma} = \sigma_T \frac{\partial \ell n(p)}{\partial \sigma} \tag{4}$$

The RMS errors for the developmental components of the horizontal velocity component tendencies are estimated from the temporal gradient of the velocity error and estimates of error contained in the advective part of the

tendencies. Thus these errors are related to the measurement errors for the velocity components,

$$\sigma_{\xi_u} = \sqrt{2}\,\sigma_u \left[\frac{1}{(\Delta t)^2} - \frac{c^2}{(\Delta S)^2} + \frac{c}{\Delta t\,\Delta S} \right]^{1/2} . \qquad (5)$$

Finally, the RMS errors for the vertical velocity are estimated through the integrated continuity equation. They are functions of the measurement error for the velocity components but can also be functions of other measured variables. The vertical velocity RMS error is found by integrating the velocity component RMS error from the surface to any level k:

$$\sigma_{\dot{\sigma}_k} = \frac{2\Delta\sigma}{\Delta S} \left(\sum_{j=1}^{k} \sigma_{u_j}^2 \right)^{1/2} . \qquad (6)$$

Table 1 shows the standard errors of observation for the winds, heights, and temperatures and the RMS errors for the other adjustable meteorological variables. Estimates for the scalar wind speed as functions of elevation angle of the balloon (Fuelberg, 1974) are given in the first two columns. The values for the 20 degree elevation angle compare favorably with the results from Hovermale's (1962) spectral decomposition of meteorological data. RMS values for heights and rawinsonde temperatures are from a composite of methods for estimating measurement error (Achtemeier, 1972). Estimates of the measurement error for the TIROS-N clear and cloudy temperature soundings are from Kidder and Achtemeier (1986).

Table 2 gives the nondimensional precision modulus weights calculated from the various functional relationships of the RMS errors from Table 1. The more accurately measured (estimated) variables receive larger values. Largest weights are accorded the geopotential height followed by the winds and temperatures. The developmental components of the local velocity tendencies receive the smallest weights. Note that weights accorded the rawinsonde temperatures between 200 and 400 mb are smaller than the corresponding weights for the satellite temperatures. Our analysis found that the mean layer satellite temperatures were more accurate than were the rawinsonde temperatures that were averaged vertically near the tropopause where large changes in stability can be found within a layer. Finally, the precision modulus weight for level 10 of the vertical velocity has been assigned a large value to require the adjusted vertical velocity to vanish at the top of the domain.

The precision modulus weights presented in Table 2 have been derived from the standard errors of observation. However, we have changed some precision moduli in order to better accomplish the objectives of this study, ie., to assess the impact temperatures measured from space-based platforms have upon a variational assimilation. First, the weights for the rawinsonde and satellite temperatures have been increased by a factor of 10. Second, the weights for the geopotential have been reduced by a factor of 10 because, as a boundary condition, it tends to force the solution toward the geopotential. Third, the weights for the developmental components of the velocity tendencies have been increased by factors of 10 to keep the variational adjustment from forcing residual error into these hypersensitive variables.

4. Evaluation of the Variational Assimilation Model

Three diagnostic criteria were defined for the evaluation of the variational assimilation model. We apply these criteria to observed fields and variational fields with and without satellite data to show that MODEL I performs as predicted by theory.

a) Satisfaction of Dynamical Constraints

This data assimilation model is derived through the variational method of undetermined Lagrange multipliers (Sasaki, 1970). The strong constraint formalism requires that the dynamical constraints; the nonlinear horizontal momentum equations, the hydrostatic equation, and an integrated form of the continuity equation, be satisfied exactly (to within truncation). Therefore, it is appropriate that the first evaluation of the variational model determine whether indeed the adjusted fields of meteorological variables are solutions of these physical equations.

In solving the Euler-Lagrange equations (see companion paper), we substituted observed or previously adjusted variables into the nonlinear terms and other terms that are products with the Rossby number or are higher order terms and treated these terms as forcing functions. This approach made the linearized equations easier to solve but several cycles with the forcing terms updated with newly adjusted variables were required for the method to converge to a solution.

In order to determine if the method indeed converges to a solution, it is necessary to average adjusted variables over two successive cycles and reintroduce them into the dynamic constraints. The residuals are computed as remainders of algebraic sums of individual terms of each constraint. The root-mean-squares (RMS) of these differences (Glahn and Lowry, 1972) vanish (constraint satisfaction) when variables at two successive cycles are unchanged. A measure of the magnitude of adjustment required to bring the initial gridded meteorological fields into variational balance is the difference between the initial RMS values (initial unadjustment) obtained by substituting unadjusted variables directly into the dynamic equations and the RMS values at each cycle. Upon dividing by the initial RMS values, the convergence at each cycle can be expressed as percent reduction of the initial unadjustment.

Figure 5 shows how the reductions of the initial RMS differences for the two horizontal momentum equations varies for each pass through the cyclical solution sequence for the eight adjustable levels of the model. The residuals are approximately halved with each cycle through the fourth cycle. The solution stabilizes to near 90-95 percent reduction of the initial unadjustment. There is small mutual adjustment between the two equations and amongst the levels with no further significant improvement in the assimilation after the fourth cycle. The reasons for the lack of continued improvement are not known with certainty, however we can not rule out two possibilities. The first possibility is cumulative truncation. Algorithms used to solve second order elliptic partial differential equations were made accurate to the fourth decimal place for computational economy. A truncation error of a few tenths of a percent is produced in the adjusted variables. The truncation error could

sum among the variables and their derivatives to increase the residuals to a few percent. The second possibility is deleterious boundary impacts. Some of the boundary conditions do not satisfy the dynamic equations (see companion paper). Each cycle through the solution sequence draws deleterious boundary effects an additional grid space into the interior of the domain. The outer three rows of grid points are not included in the model statistics. Therefore, the boundary conditions can impact upon the model statistics beginning at the fourth cycle.

The reductions of the initial unadjustment for the integrated continuity and hydrostatic equations are shown in Fig. 6. The differences for the integrated continuity equation are reduced by from 96 to 99 percent at the second cycle and improve slowly to near 100 percent by the eighth cycle. These improvements are, of course, dependent upon the magnitudes of the initial unadjustment. We set the initial vertical velocity to zero. Then the initial unadjustment is equal to the divergence integrated upward. The MODEL I cyclical solution order subjects the adjusted velocity components to a second adjustment to satisfy the integrated continuity equation. In this case, the averages of the adjusted velocity components are just averages of two solutions of the integrated continuity equation. Therefore the unadjustment should approach zero by the second cycle.

The initial unadjustments for the hydrostatic equation are halved at each cycle and the percentage reduction increases to near 100 percent by the eighth cycle.

b) Adjustment Departures from Observations

Data assimilation as treated in this paper is a two-step process. Grid point values are found by an interpolative method and then the interpolated fields are adjusted to a mutual balance subject to the satisfaction of the dynamic constraints. No direct information from the original observations is carried into the second analysis step, so the variational model treats the unadjusted initial fields as observations. Therefore, there is an implicit assumption that the initial gridded fields correctly carry the phenomena described by the observations. This assumption is not strictly true and it is necessary to grid the data accurately out to the first and second derivatives. We have modified the widely used Barnes (1964, 1973) method for gridding meteorological data to yield significant improvement in the accuracy of the gridded data and its derivatives (Achtemeier, 1988).

We compare the final analyses with the observations knowing that the variational adjustment is only one of two factors that determine the departures. However, it is the total data assimilation that is most important and these results will serve as baselines for comparisons with future improvements. These comparisons are summarized in Fig. 7 for the four observed meteorological variables: rawinsonde only data (top panels) and rawinsonde plus satellite data (bottom panels).

Consider first the solid lines in Fig. 7. Standard errors of observation for wind components, height, and temperature are listed in Table 1. This list provides the standard by which the RMS differences between the adjusted fields and the observations are compared. The solid lines in Fig. 7 give the residuals remaining after the respective standard errors are subtracted from

the RMS differences. Negative values mean that the variational analysis has brought the adjusted variables closer to the original observations than expected. Positive values mean that the adjustments have, on the whole, departed farther from the observations than expected. In interpreting these results, it must be kept in mind that the mean winter standard observational error estimates taken from Hovermale's (1962) results do not exactly express the true observational error for this case. Thus, some small departure of either sign from given values should be expected. Further, we increased the precision modulus weight for the temperature by a factor of 10 thereby decreasing the standard error by approximately three. We also divided the precision modulus for the height by 10 effectively increasing its standard error by three. These changes were made to make MODEL I more sensitive to the inclusion of satellite data and to reduce the importance of height which tends to control the solution additionally through boundary conditions.

The residuals for the temperature were mostly negative (Fig. 7a); the variational method tended toward a closer fit to the observed temperatures. This result was in accordance with the modifications in the precision moduli. The residuals for the height (Fig. 7b) are near the observational error in the middle troposphere but are approximately 5m larger near 300 mb and in the lower troposphere. Given the modifications of the heights precision moduli that effectively increased the standard error by a factor of three, the variational analysis fit the heights much more closely than expected. Possible explanations for the closeness of fit are a) the control through boundary conditions, b) the heights were already in near hydrostatic balance with temperatures, c) the heights were restored through dynamic balance with the wind field, or d) any combination of the above. Residuals for the horizontal

velocity components (Figs. 7c and 7d) show that adjustments to bring the wind field into dynamical balance with the heights and temperatures were greater than expected from theory. The magnitudes of these adjustments were greater in the lower troposphere and near 300 mb and therefore tend to follow the pattern of the height adjustments.

The residuals for the satellite case (TIROS-N mean layer temperatures replace the rawinsonde temperatures) are shown in the lower panel of Fig. 7. Only small departures from the standard observational error for temperature are found for this case (Fig. 7e). Residuals for the heights and wind (Figs. 7f - 7h), larger than they are for the rawinsonde case, represent the adjustments required to bring these variables into balance with a temperature field that was not in quasi-hydrostatic balance initially.

The dashed lines in Fig. 7 are the means of the differences between the variational fields of meteorological variables interpolated to the observation sites and the observations. Means near zero are expected unless systematic adjustment is required to achieve solution of the variational equations. Means for both the rawinsonde and satellite case temperature are near zero except for the 200 - 300 mb layer where the variational adjustment forced cooling of approximately one degree on the average. The heights are systematically lower in the middle to upper troposphere but are generally higher by approximately 10 m at 200 mb. The increased thickness of the height adjustment between 200-300 mb is a direct response to temperatures that were initially temperature for the layer and is a hydrostatic imbalance introduced by differencing across the tropopause in a 100 mb thick layer. The large magnitude of the hydrostatic imbalance is also apparent in the large initial residuals within the

hydrostatic equation at levels 2 and 3 (Fig. 6). The reduction of heights in the 300 - 500 mb layer is a compensation for the increased thickness above and must occur because the adjustment is bounded by the observed heights at the top of the model domain. Explanation for the large negative mean height residuals near 500 mb for the satellite case awaits additional information presented in the next subsection.

The large (2 - 4 m sec^{-1}) mean adjustments in the velocity components at 800 mb and 900 mb are in response to increased circulation (of both signs in these cases) around the low pressure center located over the western U.S. where the model parameterization for smoothed terrain did not allow for greater drag and channeling over the mountainous areas. The mean increase primarily in the u-component of the wind in the 300 - 400 mb layer (Figs. 7c and 7g) is the result of the variational adjustment forcing as a boundary condition, a geostrophic solution to the wind field which, fortuitously, included two jet streaks near the lateral boundaries of the analysis domain.

c) Pattern Analysis. Results for the Major Fields

Maps of heights, streamlines/isotachs, and temperatures are taken from selected levels within the variational assimilation region to better interpret the statistical results presented in subsections a) and b). Comparisons are made between patterns in the unadjusted initial fields and the adjusted fields developed by the variational analyses with rawinsonde data only (NOSAT) and with temperatures from TIROS-N substituted for rawinsonde temperatures (SAT). The analyses are done for the synoptic scale although a significant mesoscale convective system was located within the analysis domain over parts of Texas

and Oklahoma on 0000 GMT, 11 April 1979. We concentrate most of our study in the lower and middle troposphere since the greatest impact of the convective disturbance was found in the upper troposphere.

Height contours at 30 m intervals and differences between the objective and the respective variational heights at 5 m intervals are shown in Fig. 8 for level 3 (800 mb except up to 35 mb higher over the mountainous areas) and level 6 (500 mb). Small adjustments less than 10 m found with the NOSAT analyses (right panels) were expected given that the rawinsonde heights were in approximate hydrostatic balance with the rawinsonde temperatures initially. The pattern of adjustments at level 3 (lower right panel) is to increase very slightly the height gradient, hence the geostrophic wind, in the southerly flow region between the low centered over Colorado and the the ridge over southern Illinois. The adjustment at level 6 (upper right panel) is to mostly smooth the existing pattern. The trough over the Oklahoma panhandle has been diminished by about 5 m and the ridge over Minnesota by about 10 m. The ridge over southern Illinois has been strengthened by about 5 m. The level 3 SAT analysis (lower left panel) strengthened the ridge over the Great Lakes and filled the Colorado low by 15 m. The adjustment pattern weakens the height gradient, hence the geostrophic circulation, to the west of the low. At level 6 (upper left panel), the SAT analysis increased height gradients across the central U.S. by deepening the Colorado low and broadening the trough into the Plains states while maintaining heights in the ridge to the east at unadjusted analysis levels. The trough over the Oklahoma was locally deepened up to 25 m.

The impact of the SAT analysis upon the level 6 wind field was to increase the circulation about the Colorado cyclone. The vector differences

between the SAT and unadjusted initial wind fields in Fig. 9 are aligned with the height field. Increases in circulation were 5 m sec^{-1} west of the low and greater than 10 m sec^{-1} over Texas southeast of the low.

An unfortunate circumstance with the satellite data was the tendency for large blocks of no data to coincide with key areas in the analysis. Fig. 3 shows that one such block covered the southwestern part of the analysis grid from Oklahoma and Texas westward to California. Several of the extreme features of the SAT adjustment are located within or along the boundaries of the data void. Although aliasing of features into data voids and phase shifting of patterns within data-rich areas near the boundaries of the data field can have deleterious impacts upon an analysis (Achtemeier, 1986), the SAT adjustment patterns found within the data void extend far into the interior of the data-rich area.

An example of poor performance of the variational assimilation near a mesoscale phenomenon is the level 8 (300 mb) wind field shown in Fig. 10. Accurately drawn objective streamlines (Achtemeier, 1979) and isotachs reveal in Fig. 10a a prominent wind maximum over Kansas (actually smoothed by 12 m s^{-1}) in the initial wind field. It is a typical pattern and location of a narrow, intense jet streak along the northwest edge of the mesoscale convective system (Fritsch and Maddox, 1981; Maddox, et al., 1981). Both the NOSAT and SAT analyses (Figs. 10b and 10c), which are weighted toward the synoptic patterns of temperatures and heights replace it with a larger scale jet steak that increases southwestward toward Texas. A relative increase of the precision modulus weights for the wind field will restore this feature.

d) Pattern Analysis: Results for the Hypersensitive Variables

The variational assimilation has significantly adjusted height, temperature, and wind velocity in order that they be solutions of the dynamic constraints. However, these modifications can cause large and physically unrealistic changes in other important meteorological variables such as vorticity, divergence, and vertical velocity that are derived from derivatives of the basic variables. In addition, the local tendencies of the horizontal velocity components are sensitive to small errors in the basic variables since they are determined from the arithmetic sum of the other terms of the horizontal momentum equations. The patterns of these hypersensitive variables must be physically realistic when compared with other data sets such as cloud fields, precipitation, and independent measurements of the variable. Thus, the hypersensitive variables provide a critical test of the MODEL I dynamic assimilation.

Patterns of relative vorticity for the unadjusted wind field and the NOSAT and SAT variational assimilations are shown in Fig. 11 for level 6 (500 mb). The primary difference is that the vorticity gradient, identifying the area of positive vorticity advection (PVA) and upward vertical velocity, over the Texas panhandle (Fig. 11a) has been shifted northeastward over Oklahoma and Kansas to locations coincident with the mesoscale convective system.

The vertical velocity patterns at level 3 (800 mb) in all three comparative fields (Fig. 12) are located favorably with the PVA patterns; the magnitudes of the variational fields being smoothed by approximately 30 percent. Please note that the vertical velocities for the unadjusted wind

field have been modified by the O'Brien (1970) variational method. The large 18 cm sec^{-1} vertical velocity center over the Texas panhandle at level 6 (Fig. 13a) compares favorably in orientation with the precipitation associated with the mesoscale convective system over Oklahoma and Kansas. It picks up the extension of strong thunderstorms over southern Missouri but misses the strong storms over Louisiana. The initial vertical velocities differ considerably from the variational adjustment fields (Figs. 13b and 13c) which are mostly intensifications of the patterns found at level 3. The variational vertical velocities are better aligned with the pattern of severe convection over Oklahoma and Texas, they pick up the strong storms over Louisiana but miss the storms over Missouri.

The initial and variational vertical velocities compare favorably with the vertical velocities from the NMC LFM II numerical prediction model (Fig. 14) which picked up the strong storms over Louisiana but placed the storms over the Plains within a broad area of weak upward motion thus greatly underestimating the strength of the vertical velocities within the mesoscale convective system.

The methodology for partitioning the local tendencies of u and v into developmental and advective components was presented in the companion paper. Once the variational assimilation is completed, the developmental components are recombined with the advective components, redimensionalized, and expressed as 3-hr changes. These 3-hr "adjustment" tendencies in the velocity components can be compared with the changes observed from 3-hr rawinsonde data collected over the central part of the U. S. as part of the NASA AVE/SESAME project (see grid in Fig. 3). The comparisons also include 3-hr tendencies calculated from

substitution of unadjusted variables into the horizontal momentum equations. In making these comparisons, we make the assumption that the observed 3-hr tendencies represent "ground truth". This assumption is not strictly true for the following reasons. First, even though we have gridded only 3-hr tendencies taken from data collected at standard NWS observing sites, it is certain that some of the observations, either at 0000 GMT or at 0300 GMT, contain significant local scale "noise". A major mesocale convective system, located near the center of the SESAME network, significantly perturbed the synoptic scale wind field in the upper troposphere, and caused us to restrict our analysis to the middle and lower troposphere where the local scale wind field perturbations were much smaller. Second, the 3-hr tendencies calculated from the unadjusted and MODEL I fields of meteorological variables are synoptic and are therefore centered at 0000 GMT. There is no reason to assume that these tendencies should have close correspondence with the ground truth tendencies that are calculated over the 3-hr interval from 0000-0300 GMT and are therefore centered at 0130 GMT. And third, there is no reason to assume that the synoptic tendencies should have any correspondence with the 3-hr tendencies unless the period of the weather systems is three hours or greater.

Fig. 15 shows fields of the diagnosed 3-hr velocity component tendencies at level 3 (800 mb). The observed change in the u-component of the wind during the period 0000 GMT and 0300 GMT (Fig. 15a) is a center of increasing westerly winds over Oklahoma and a zone, smaller in magnitude, of decreasing westerly winds from Iowa through Alabama (right edge of grid). Both SAT and NOSAT variational analyses accurately located the center over Oklahoma albeit with slightly decreased magnitudes (Figs. 15b and 15c). The two variational analyses also located the zone of negative tendencies but the magnitudes were

much reduced. In general, the variational 3-hr u-component tendencies seem highly accurate, especially when they are compared with the 3-hr u-component tendencies calculated from the unadjusted fields of meteorological variables (Fig. 15d). These tendency patterns show little resemblance to the observed tendencies in either magnitudes or signs. The results for the v-component are encouraging also. The patterns of observed v-tendencies (Fig. 15e) show two centers, one with decreasing v over the western Plains and the other with increasing v over the mid-Mississippi valley. Both variational analyses produce similar patterns albeit the gradients are weakened and shifted southwestward over Kansas and Oklahoma (Figs. 15f and 15g). The unadjusted v-tendency (Fig. 15 h) shows no correspondence with the observed patterns.

Fig. 16a shows a potent mesoscale pattern in the observed u-component tendencies at level 6. The 12 m s^{-1} change over Oklahoma is smoothed from a 25 m s^{-1} change over 3 hours at the Oklahoma City observing site. Oklahoma City was located deep within the mesoscale convective system at 0000 GMT (Note cloud field over Oklahoma in Fig. 2) and the relatively light winds observed there appear in the truncated jet streak at level 7 (300 mb) at 0000 GMT (Fig. 10a). Both variational analyses (Figs. 16b and 16c) place large positive centers over Oklahoma with the SAT analysis outperforming the NOSAT analysis. The large negative center in the observed field over Missouri/Illinois was absent from both variational analyses. No correspondence between the observed and unadjusted tendencies (Fig. 16d) was apparent. Level 6 v-component tendencies were accurately reproduced by the variational analyses (Figs. 16e-16g). There was no correspondence with the unadjusted tendencies (Fig. 16h).

The variational tendencies shown in Fig. 15 and 16 are similar in many patterns to the observed tendencies but also show significant differences, particularly with respect to a large negative 3-hour tendency in the level 6 u-component over Missouri/Illinois. Although the variational tendencies are significantly improved over the unadjusted tendencies, the question remains whether the differences at level 6 can be explained by mesoscale contamination of the 0000 GMT wind field or by negative impacts brought upon the u-component tendency by the variational adjustment. Since the velocity component tendencies are diagnosed by the variational method, it is a simple matter to extrapolate (forecast) forward to the 0300 wind field and compare with the observed 0300 winds. If the observed 0000 GMT wind field contained a significant mesoscale perturbation that was filtered from the variational analyses, then it is possible that the forecast variational wind field will be closer to the observed 0300 GMT wind field than implied by the large differences in the 3-hr tendencies.

Fig. 17 shows the forecast results for level 3 (800 mb). Strong west winds over New Mexico (lower left corner of grid) in Fig. 17a have expanded eastward over Texas and Oklahoma at 0300 GMT (Fig. 17b). An area of strong east winds over Nebraska (upper left corner of grid) also has expanded eastward. Both variational analyses show the same pattern shifts (Figs. 17c and 17d). The NOSAT analysis has accurately located all major features of the 0300 wind field including the location of the magnitude of the east wind over Iowa where there existed a 4 m sec^{-1} difference over 3 hours in the u-component tendencies (Fig. 15a and 15c). The pattern of southerly winds shifted eastward and increased in magnitude over the 3-hour period (Figs. 17e and 17f). Both variational analyses accurately reproduced the 0300 GMT

patterns of v-components. A notable exception was the premature movement of northerly winds into the western edge of the grid.

Fig. 18a and 18b reveal the movement of strong west winds into Texas and Oklahoma and the decline of strong west winds over Missouri and Illinois. Winds over southwestern Kansas and western Oklahoma also switched from easterly to westerly. Recall the large center over Missouri/Illinois of negative 3-hr u-component tendencies in Fig. 16a. The predictions from the variational analyses, which produced no large u-component tendencies in the area, have almost reproduced the 0300 GMT wind field (Figs. 18c and 18d). Both variational analyses have overestimated the strength of the westerly flow over Texas, with the NOSAT analysis giving the best approximation to the observed wind field. The 3-hr v-component tendencies for the observed and variational analyses were not large at level 6 (Fig. 16 e-h). Therefore, the differences between the patterns at 0300 GMT are mostly the differences in the patterns at 0000 GMT. The variational v-components were adjusted to approximately 5 m sec^{-1} larger than the observed.

5. Discussion

We have evaluated a diagnostic multivariate data assimilation method described in a companion paper (Achtemeier and Ochs, 1988). The method is designed to incorporate data from diverse sources and, in particular, to mesh observations from space-based platforms with those from more traditional immersion techniques. Meteorological data are weighted according to relative "measurement" errors and blended into a data set that satisfies the two nonlinear horizontal momentum equations, the hydrostatic equation, and an

integrated continuity equation for a dry atmosphere as dynamical constraints. A nonlinear vertical coordinate allows for the easy incorporation of TIROS-N mean layer temperatures.

The purpose of this paper was to assess the performance of the variational assimilation with and without satellite data in comparison with initial analyses and the observations. We have used three diagnostic criteria which measure a) the extent to which the assimilated fields satisfy the dynamical constraints, b) the extent to which the assimilated fields depart from the observations, and c) the extent to which the assimilated fields are realistic as determined by pattern analysis. The last criterion requires that the signs, magnitudes, and patterns of the hypersensitive vertical velocity and local tendencies of the horizontal velocity components be physically consistent with respect to the larger scale weather systems.

The intense cyclogenesis of 0000 GMT 11 April 1979 was selected for the case study because TIROS-N temperature soundings coexist with NASA AVE/SESAME 3-hr rawinsonde data over a large area of the central United States; the latter data set was required to provide verification for the diagnosed 3-hr local tendencies of the horizontal velocity components.

A summary of the results of this study follows.

(Results from the evaluation of constraint satisfaction.)

1. The residuals for the nonlinear horizontal momentum equations were approximately halved with each cycle through the fourth cycle. The solution

stabilized to near 90-95 percent reduction of the initial unadjustment and there was small mutual adjustment between the two equations and amongst the levels with no further significant improvement in the assimilation after the fourth cycle.

2. The residuals for the integrated continuity equation were reduced 96 to 99 percent at the second cycle and were reduced to near 100 percent by the eighth cycle.

3. The initial unadjustments for the hydrostatic equation were halved at each cycle and the percentage reduction increased to near 100 percent by the eighth cycle.

(Results from comparisons of variational analyses with observations.)

4. The SAT and NOSAT adjusted temperatures tended toward a close fit to the observed temperatures in accordance with the design for this study. Root-mean-square differences between observed and analyzed temperatures were approximately one degree Kelvin less than the standard error of observation for the NOSAT analyses and about equal to the standard error for the temperature for the SAT analyses.

5. The heights were fit much more closely than expected by both variational adjustments. Possible explanations for the closeness of fit are a) the control through boundary conditions, b) the heights were already in near hydrostatic balance with temperatures, c) the heights were restored through dynamic balance with the wind field.

6. Analysis of the means of the differences between the variational fields of meteorological variables interpolated to the observation sites and the observations revealed that systematic adjustment was required near and above the tropopause to achieve solution of the variational equations. Thicknesses of the 200 - 300 mb layer were increased by approximately 10 - 15 meters.

(Results from pattern analysis for the major fields.)

7. In general, adjustments in the heights in the middle troposphere by NOSAT smoothed the initial analyses of the troughs and ridges by 5 - 10 meters. The SAT analysis strengthened these patterns. The SAT analyses deepened the major low by approximately 10 m, increased the heights and height gradients west of the low, and locally deepened a weak trough over the Oklahoma by up to 25 m.

8. The SAT analysis increased the circulation about the Colorado cyclone by 5 m s^{-1} west of the low and by more than 10 m s^{-1} over Texas, southeast of the low.

9. Both the NOSAT and SAT analyses, weighted to force the wind field toward the mass field, filtered out a mesoscale jet streak and replaced it with a larger scale jet steak that better fit the synoptic scale situation.

(Results for pattern analysis for the hypersensitive variables.)

10. The vertical velocity patterns at level 3 (800 mb) in all three comparative fields were located favorably with the patterns of positive

vorticity advection. In the middle troposphere, the patterns and magnitudes of the fields of both initial vertical velocity and SAT and NOSAT vertical velocity compared favorably with parts of precipitation patterns located over Oklahoma, Missouri, and Louisiana. SAT and NOSAT vertical velocities were superior to the vertical velocities obtained from the NMC LFM II numerical prediction model.

11. In general, the diagnosed local tendencies of the horizontal velocity components compared favorably in both signs and magnitudes with the observed 3-hr tendencies within the lower and middle troposphere. The upper tropospheric wind field contained circulations from an intense mesoscale convective system and comparative studies were not attempted. By contrast, 3-hr tendencies calculated from the unadjusted meteorological variables showed little or no correspondence with the observed tendencies.

12. The 3-hr velocity component tendencies were combined with the velocity components at the synoptic time to develop forecasts of the 0300 GMT wind field. The predictions based on both variational analyses were accurate in the movement, location, and intensification of important wind field features in the lower and middle troposphere.

Upon further theoretical analysis, we have come to regard the adjustment for the divergent part of the wind as the "weak link" in this variational assimilation model. First order terms that contain the divergence adjustment cancel out in the cyclical solution formulations. The divergence adjustment must then be carried in second order terms involving other variables. Our solution for this problem has been to require the adjusted horizontal velocity

components to satisfy the continuity equation constraint after each cycle - a variational model within a variational model - then allow for the second order terms and the readjusted velocity components to "nudge" the solution toward the desired dynamic balance. After analysis of this and another case study, we are not yet convinced that the required final dynamic balance is obtained after eight cycles although there was slow convergence. A more complete assessment of this problem awaits the inclusion of the thermodynamic equation as the fifth constraint, a subject of ongoing research.

One of the most significant, and perhaps most puzzling, results of this study is the ability of the variational assimilation to accurately diagnose the tendencies of the horizontal velocity components and to accurately predict the 0300 GMT wind field therefrom. Accurate diagnosis of local tendencies has not, to our knowledge, been performed successfully apart from the initialization of numerical prediction models. The puzzling aspect is that there are a number of reasons why there should have been no correspondence at all. The dominant weather system over the SESAME I network, over which the observed velocity tendencies were calculated, was an intense mesoscale convective system. For reasons already mentioned, this disturbance was greatly smoothed by the variational assimilations. This resulted in rather large adjustments in the 0000 GMT wind field yet the 3-hr forecast wind fields were quite accurate. Was this result fortuitous?

Given the complexity of the variational assimilation, the possibility of achieving accuracy by chance seems remote. An alternative explanation is that the 0000 GMT wind field was perturbed by the mesoscale disturbance but the 0300 GMT wind field was not, at least at the locations of the rawinsonde

observations. The variational assimilation filtered out the unresolvable variations in the 0000 GMT wind field caused by the mesoscale convective system thus leaving the synoptic scale circulations. The local tendencies of the velocity components diagnosed from the synoptic scale adjustment, were accurate predictors of the synoptic scale wind field three hours later.

The diagnosis of the velocity component tendencies was a crucial test for the variational assimilation. The encouraging results from this study await confirmation with additional case studies and the extension of variational MODEL I to include the thermodynamic equation.

Acknowledgments.

This work was supported by the National Aeronautics and Space Administration (NASA) under Contract NAS8-34902 and Grant NAG8-059. The programming efforts of Mrs. Julia Chen (MODEL I) and Ms. Donna Isard (figures) are gratefully acknowledged.

REFERENCES

Achtemeier, G. L., 1988: Modification of a Successive Corrections Objective Analysis for Improved Higher Order Calculations. (Submitted to Monthly Weather Review)

_____, 1987: On the concept of varying influence radii for a successive corrections objective analysis. Mon. Wea. Rev., 115, 1760-1771.

_____, 1986: The impact of data boundaries upon a successive corrections objective analysis of limited-area data sets. Mon. Wea. Rev., 114, 40-49.

_____, 1979. Evaluation of operational objective streamline methods. Mon. Wea. Rev. 107, 198-206.

_____, 1975: On the Initialization problem: A variational adjustment method. Mon. Wea. Rev., 103, 1090-1103.

_____,1972: Variational initialization of atmospheric fields - a quasi-geostrophic diagnostic model. Ph.D. Dissertation, Tallahassee, Florida State University, 101-103.

_____, and H. T. Ochs, 1988: A multivariate variational objective analysis - assimilation method. Part 1: Development of the basic model. (Submitted to Tellus)

Barnes, S. L., 1973: Mesoscale objective analysis using weighted time-series observations. NOAA Tech. Memo. ERL NSSL-62, National Severe Storms Laboratory, Norman, OK 73069, 60 pp. (NTIS COM-73-10781).

_____, 1964: A technique for maximizing details in numerical weather map analysis. J. Appl. Meteor., 3, 396-409.

Bratseth, A. M., 1986: Statistical interpolation by means of successive corrections. Tellus, 38A, 439-447.

Fritsch, J. M., and R. A. Maddox, 1981: Convectively driven mesoscale weather systems aloft. Part I: Observations. J. Appl. Meteor., 20, 9-19.

Fuelberg, H. E., 1974: Reduction and error analysis of the AVE II pilot experiment data. NASA CR-120496, Marshall Space Flight Center, Alabama, p. 60

Glahn, H. R., and D. A. Lowry, 1972: The use of model output statistics (MOS) in objective weather forecasting. J. Appl. Meteor., 11., 1203-1211.

Gruber, A., and C.D. Watkins, 1982: Statistical assessment of the quality of TIROS-N and NOAA-6 satellite soundings. Mon. Wea. Rev., 110, 867-876.

Hovermale, J. B., 1962: A comparison of data accuracy in the troposphere and in the stratosphere. Dept. Meteorology, Penn. State Univ., Contract AF

19-(604)-6261, Rept. No. 2.

Kidder, S. Q., and G. L. Achtemeier, 1986: Day-night variation in operationally-retrieved TOVS temperature biases. Mon. Wea. Rev., 114, 1775-1778.

Krishnamurti, T. N., 1968: A diagnostic balance model for studies of weather systems of low and high latitudes. Rossby number less than one. Mon. Wea. Rev., 96, 197-207.

Maddox, R. A., D. J. Perkey, and J. M. Frisch, 1981: Evolution of upper tropospheric features during the development of a mesoscale convective complex. J. Atmos. Sci., 38, 1664-1674.

Mesinger, G., and A. Arakawa, 1976: Numerical methods used in atmospheric models. Vol. 1, GARP Publications Series No. 17, p47.

O'Brien, J.J., 1970: Alternative solutions to the classical vertical velocity problem. J. Appl. Meteor., 9, 197-203.

Otto-Bliesner, B., D. P. Baumhefner, T. W. Schlatter, and R. Bleck, 1977: A comparison of several data analysis schemes over a data-rich region. Mon. Wea. Rev., 105, 1083-1091.

Phillips, N., L. McMillin, A. Gruber, and D. Wark, 1979: An evaluation of early operational temperature soundings from TIROS-N. Bull. Amer. Meteor. Soc., 60, 1188-1197.

Sasaki, Y., 1958: An objective analysis based upon the variational method. J. Meteor. Soc. Japan, 36, 77-88.

_____, 1970: Some basic formalisms in numerical variational analysis. Mon. Wea. Rev., 98, 875-883.

Schlatter, T.W., 1981: An assessment of operational TIROS-N temperature retrievals over the United States. Mon. Wea. Rev., 109, 110-119.

_____, G. W. Branstator, and L. G. Thiel, 1976: Testing a global multivariate statistical objective analysis scheme with observed data. Mon. Wea. Rev., 104, 765-783.

Whittaker, E., and G. Robinson, 1926: The Calculus of Observations, (2nd Edition). London, Blackie and Son, Ltd., p.176.

Table 1

Nondimensional standard errors of observation for wind, height, and temperature and RMS errors for other adjustable meteorological variables.

Model Level	Pressure (mb)	VARIABLE u_{20}	u_{40}	H	$\delta H/\delta x$	$\delta H/\delta\sigma$	Mean Temperature Rawin	T(cl)	T(cy)	σ	ε_u
										0.00	
10	100	0.45	0.23	0.25	0.71						
						3.68	0.59	0.57	0.57	2.13	6.98
9	200	0.45	0.23	0.20	0.56						
						3.21	0.88	0.70	0.76	1.88	6.98
8	300	0.42	0.21	0.18	0.51						
						2.28	0.88	0.59	0.79	1.64	6.51
7	400	0.36	0.18	0.15	0.42						
						1.53	0.76	0.56	0.76	1.43	5.58
6	500	0.32	0.16	0.12	0.33						
						0.97	0.59	0.53	0.70	1.24	4.65
5	600	0.30	0.15	0.09	0.26						
						0.61	0.44	0.50	0.67	1.04	4.34
4	700	0.28	0.14	0.08	0.22						
						0.53	0.44	0.53	0.70	0.84	3.72
3	800	0.24	0.12	0.07	0.20						
						0.47	0.44	0.59	0.82	0.64	3.26
2	900	0.21	0.11	0.06	0.18						
						0.42	0.44	0.70	1.03	0.44	3.10
1	1000	0.20	0.10	0.06	0.17						

Table 2

Nondimensional precision modulus weights for variational assimilation.

Model Level	Pressure (mb)	VARIABLE u_{20}	H	$\delta H/\delta x$	$\delta H/\delta\sigma$	Mean Temperature Rawin	T(cl)	T(cy)	σ	ε_u
									10^6	
10	100	2.5	8.0	1.0						
					0.04	1.4	1.5	1.5	0.11	0.01
9	200	2.5	12.5	1.6						
					0.05	0.6	1.0	0.9	0.14	0.01
8	300	2.8	15.4	1.9						
					0.10	0.6	1.4	0.8	0.19	0.01
7	400	3.9	22.2	2.8						
					0.21	0.9	1.6	0.9	0.24	0.02
6	500	4.9	34.7	4.6						
					0.53	1.4	1.8	1.0	0.33	0.02
5	600	5.6	61.7	7.4						
					1.34	2.6	2.0	1.1	0.46	0.03
4	700	6.4	78.1	10.3						
					1.78	2.6	1.8	1.0	0.71	0.04
3	800	8.7	102.0	12.5						
					2.26	2.6	1.4	0.7	1.22	0.05
2	900	11.3	138.9	15.4						
					2.83	2.6	1.0	0.5	2.58	0.05
1	1000	12.5	138.9	17.3						

FIGURE CAPTIONS

Fig. 1. The NMC analysis of the 500 mb heights at 0000 GMT, 11 April 1979 showing a major trough over the southwest U.S.

Fig. 2. GOES-EAST visible distribution of clouds associated with the major trough at 0000 GMT, 11 April 1979.

Fig. 3. The distribution of a) rawinsonde stations and b) TIROS-N temperature soundings over the analysis grid (solid rectangle), evaluation grid (large dashed rectangle), and SESAME I network (small dashed rectangle).

Fig. 4. The grid template for the variational assimilation model.

Fig. 5. Residual reduction as a function of cycle for the u-component (top panel) and v-component (bottom panel) dynamic constraints.

Fig. 6. Residual reduction as a function of cycle for the integrated continuity equation (top panel) and hydrostatic equation (bottom panel) dynamic constraints.

Fig. 7. RMS differences between variational analyses and observations after removal of standard observation error (solid lines) and means of differences between variational analyses and observations (dashed lines).

Fig. 8. Heights (dm) and differences between adjusted and unadjusted heights (dashed lines) in meters for SAT (left panels) and NOSAT (right panels) for level 6 (500 mb) (top panels) and level 3 (800 mb) (bottom panels).

Fig. 9. Vector differences between SAT and initial analyses for level 6 (500 mb).

Fig. 10. a) unadjusted, b) SAT, and c) NOSAT streamline and isotachs (m sec^{-1}) of the level 8 (300 mb) wind field.

Fig. 11. a) unadjusted, b) SAT, and c) NOSAT relative vorticities for level 6 (500 mb).

Fig. 12. a) unadjusted, b) SAT, and c) NOSAT vertical velocities (cm sec^{-1}) at level 3 (800 mb). Precipitation areas are stippled.

Fig. 13. Same as Fig. 11 but at level 6 (500 mb).

Fig. 14. Vertical velocity (solid lines) in cm sec^{-1} for 0000 GMT 11 April 1979 from the NMC LFM II numerical prediction model.

Fig. 15. Velocity component tendencies at level 3 (800 mb) in m sec^{-1} 3-hr^{-1} for the u-component (left panels) and the v-component (right panels). (a and e) observed, (b and f) SAT, (c and g) NOSAT, and (d and h) unadjusted.

Fig. 16. Same as Fig. 15 but for level 6 (500 mb).

Fig. 17. Observed and predicted u-components (left panels) and v-components

(right panels) for level 3 (800 mb). (a and e) observed at 0000 GMT, (b and f) observed at 0300 GMT, (c and g) SAT predicted valid at 0300 GMT, and (d and h) NOSAT predicted valid at 0300 GMT.

Fig. 18. Same as Fig. 17 but for level 6 (500 mb).

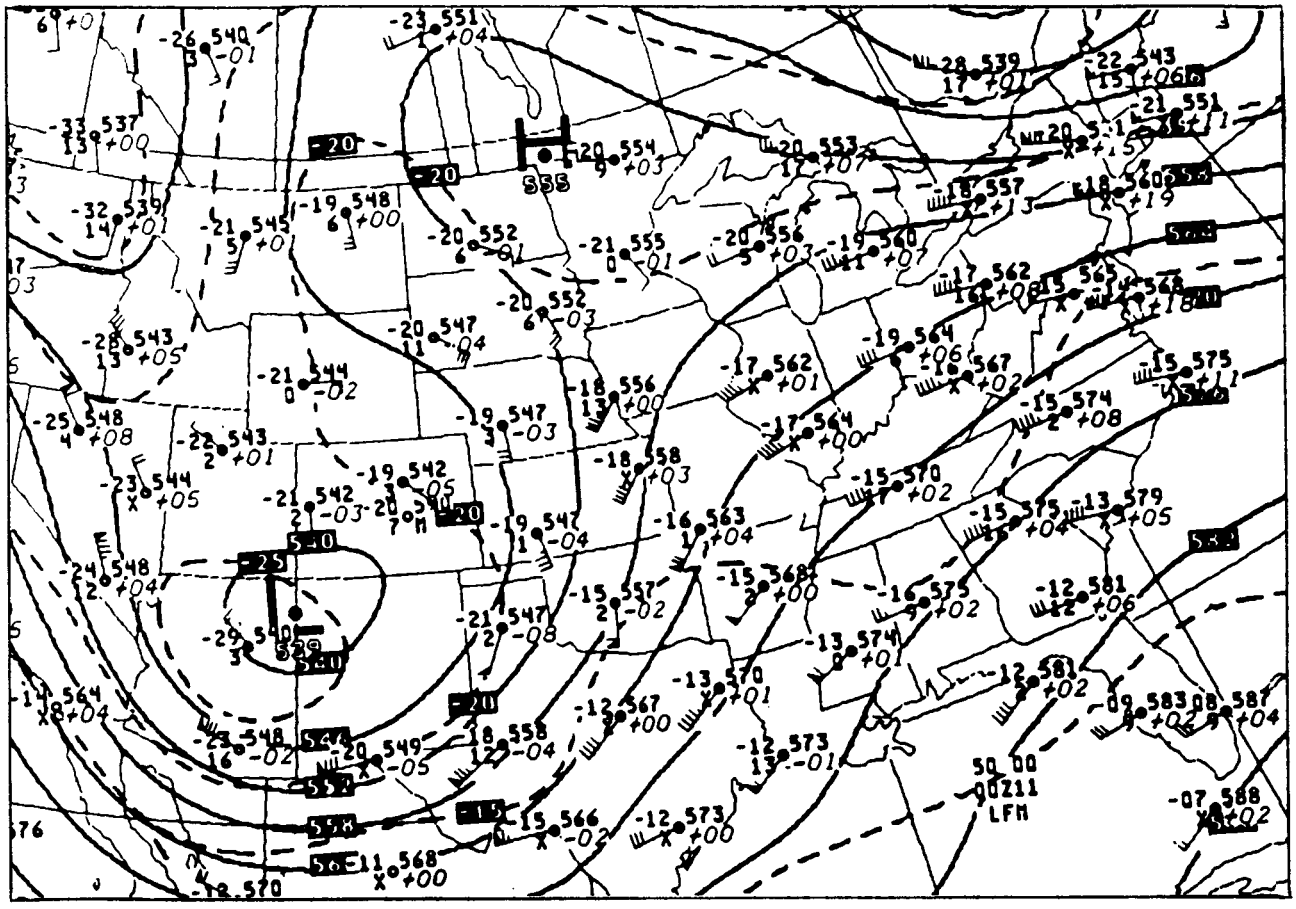

Fig 1

Fig. 2

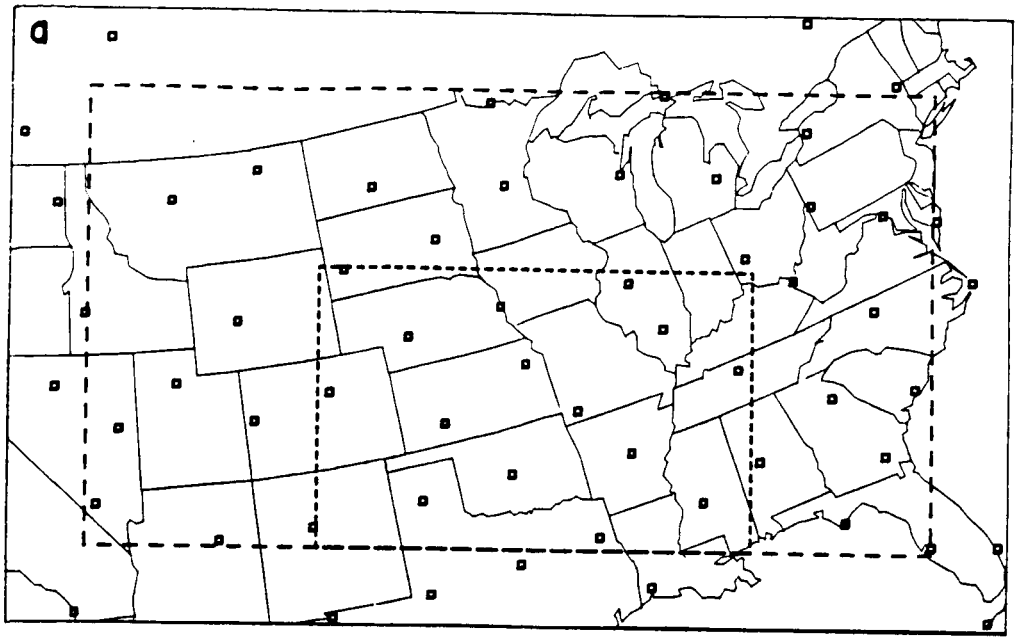

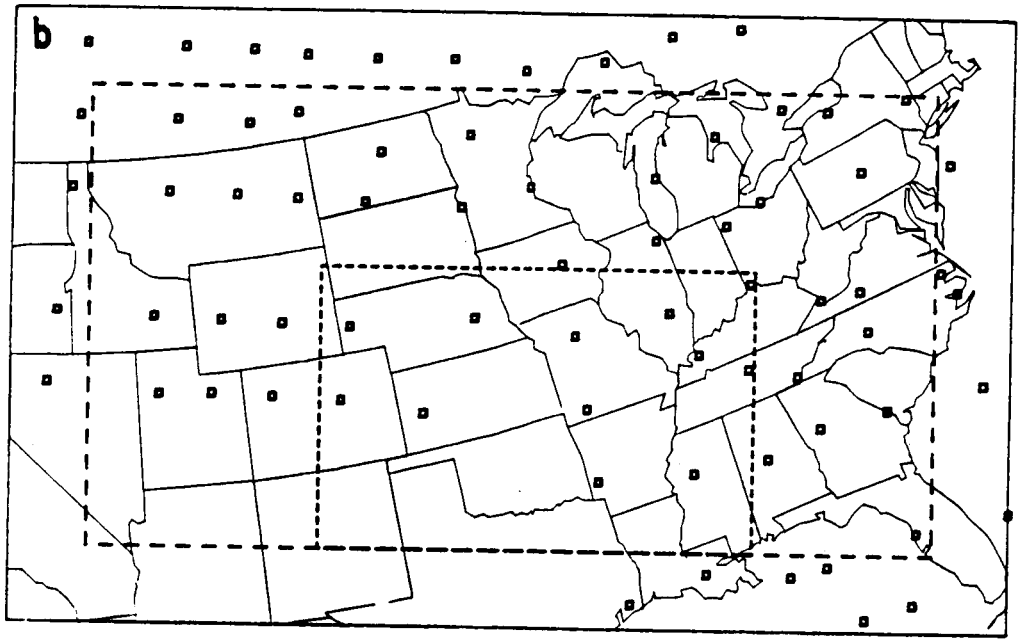

Fig 3

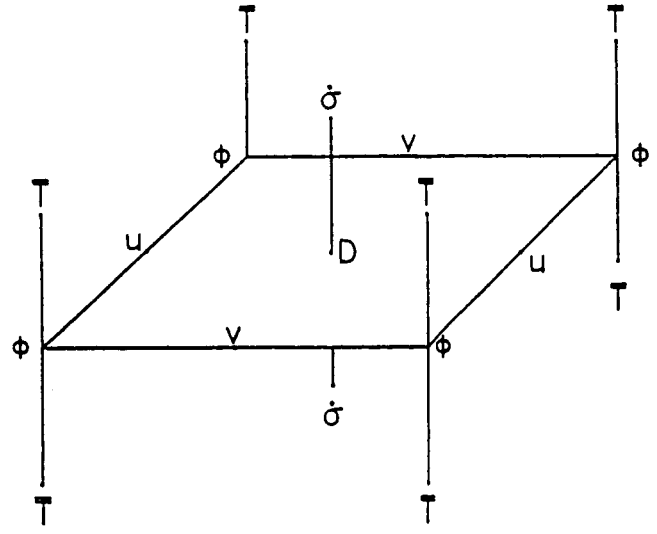

Fig 4

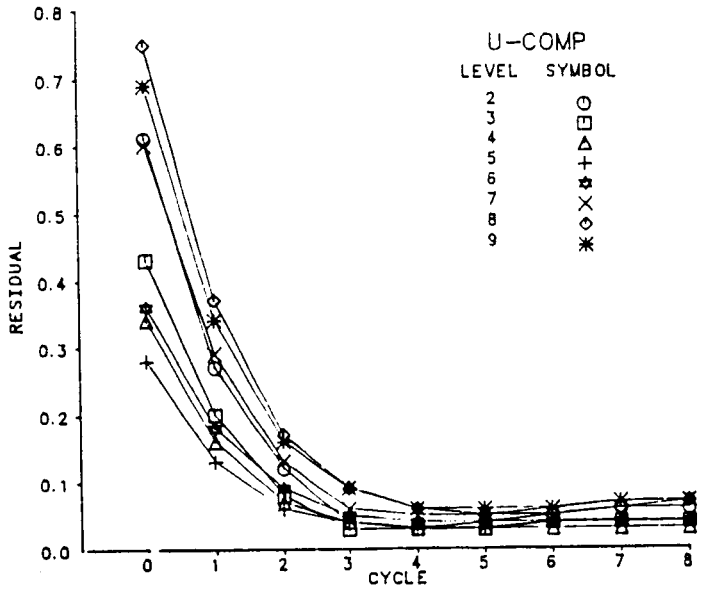

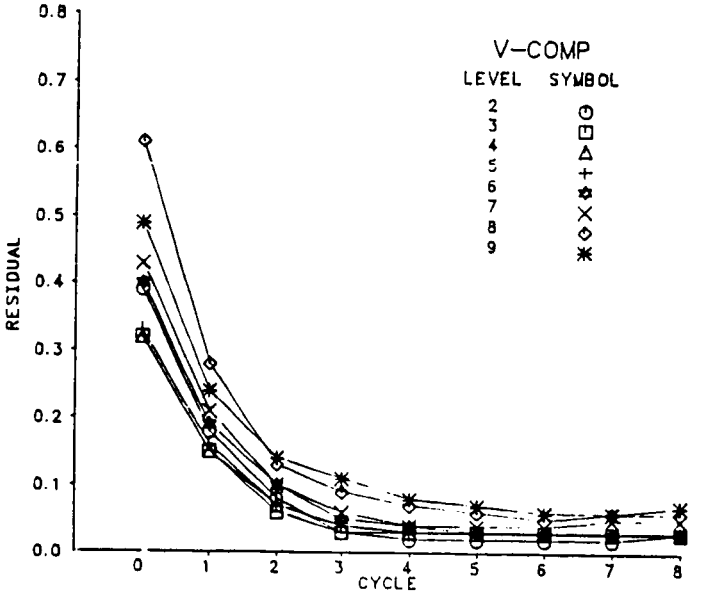

Fig. 5

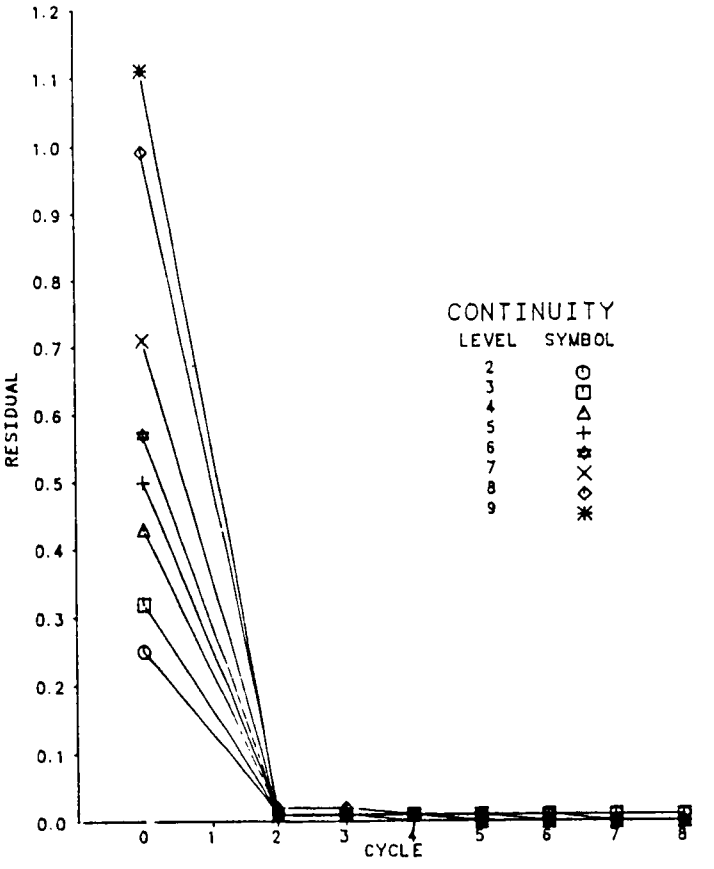
RESIDUAL
CYCLE
CONTINUITY
LEVEL SYMBOL
2
3
4
5
6
7
8
9

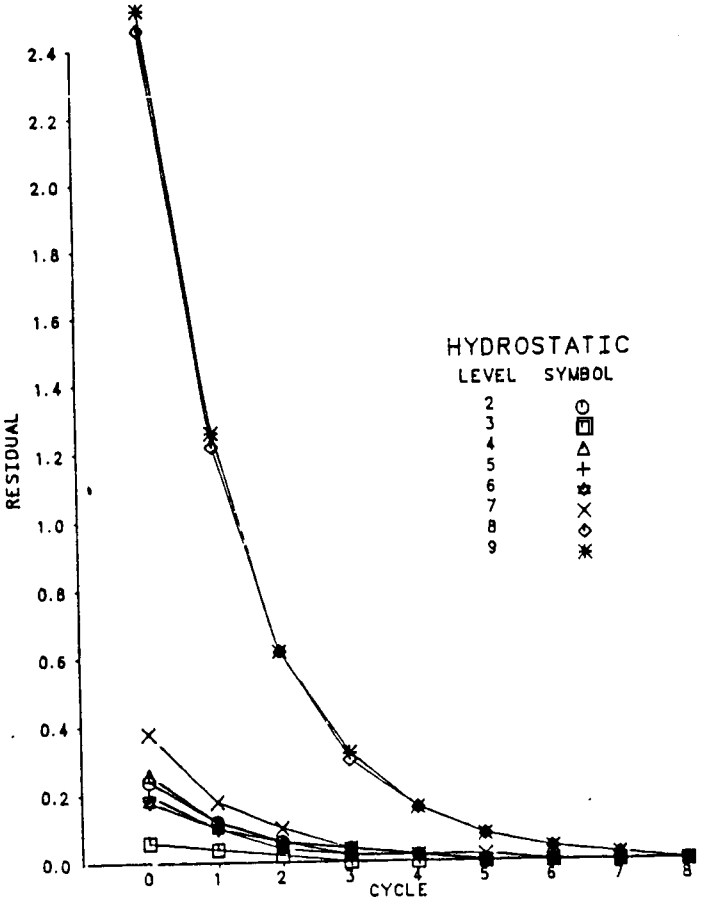
RESIDUAL
CYCLE
HYDROSTATIC
LEVEL SYMBOL
2
3
4
5
6
7
8
9

Fig 6

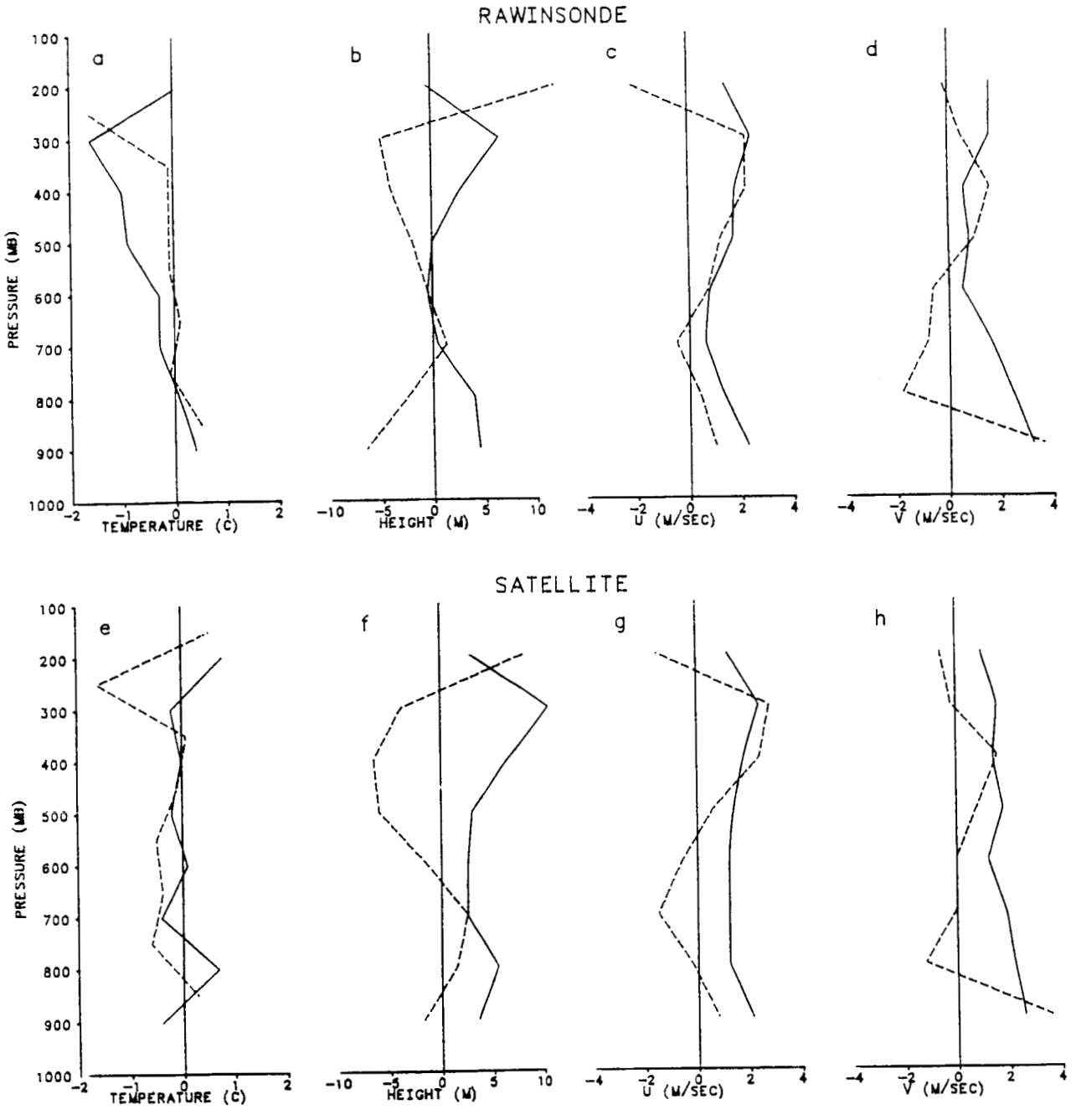
RAWINSONDE
a
b
c
d
PRESSURE (MB)
100
200
300
400
500
600
700
800
900
1000
TEMPERATURE (C)
HEIGHT (M)
U (M/SEC)
V (M/SEC)
SATELLITE
e
f
g
h

Fig. 7

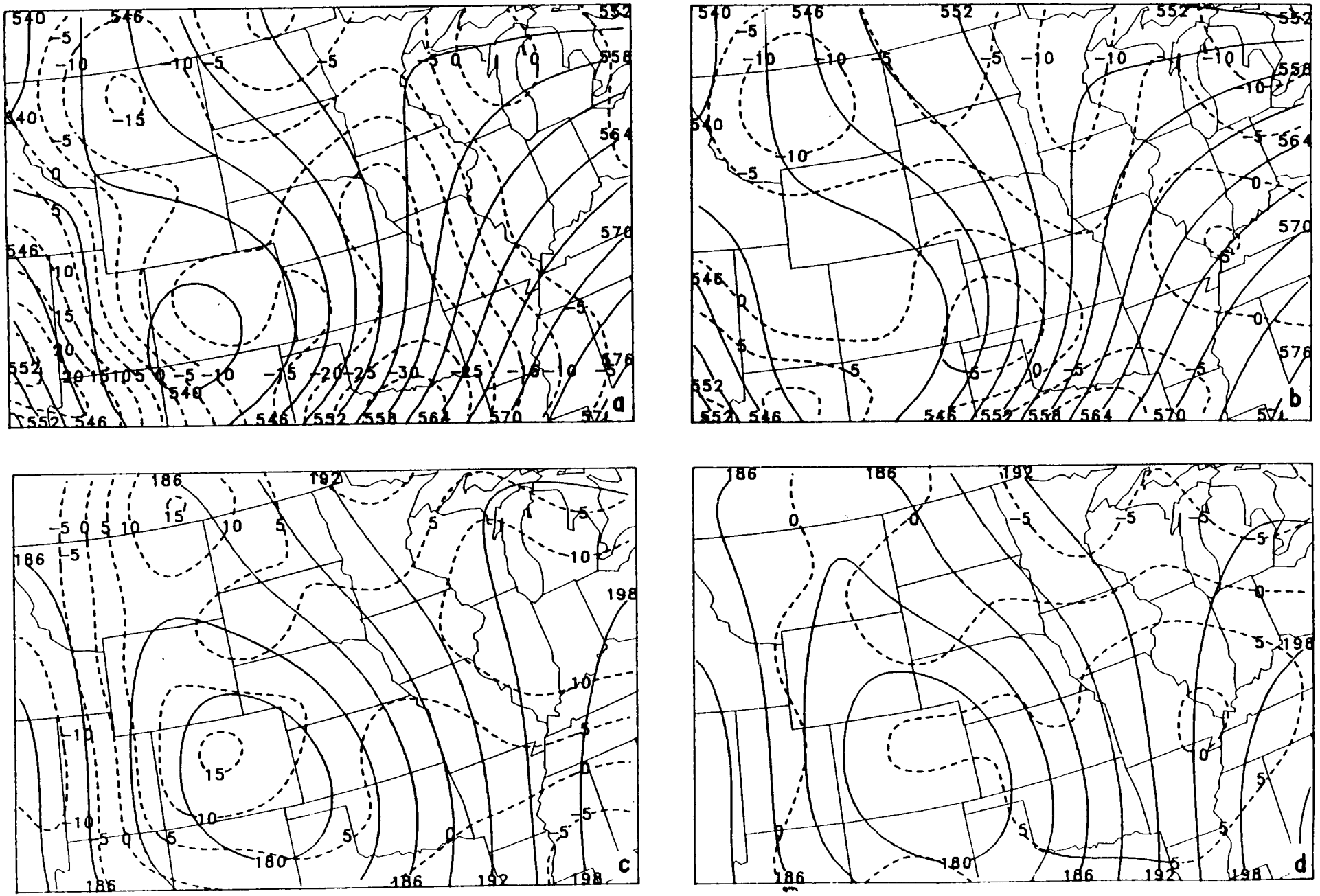

Fig. 8

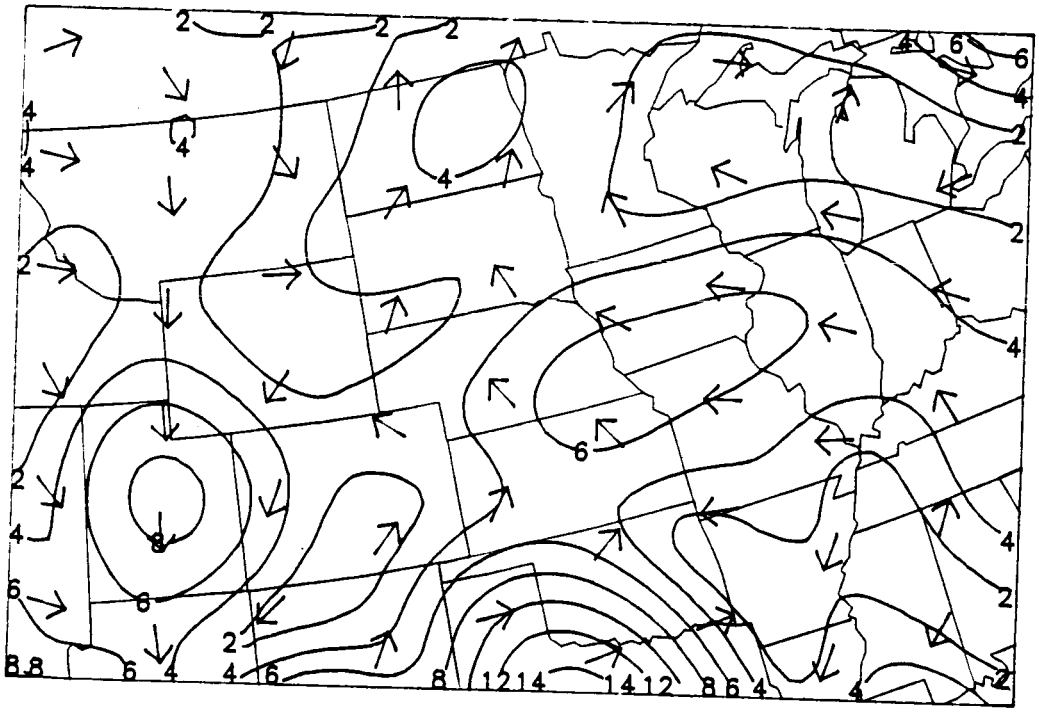

Fig. 9

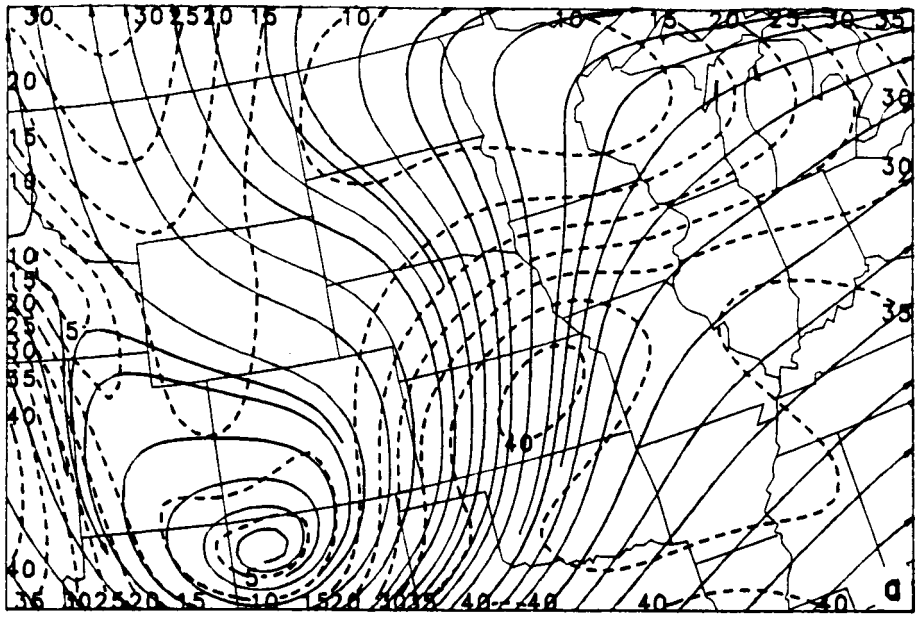

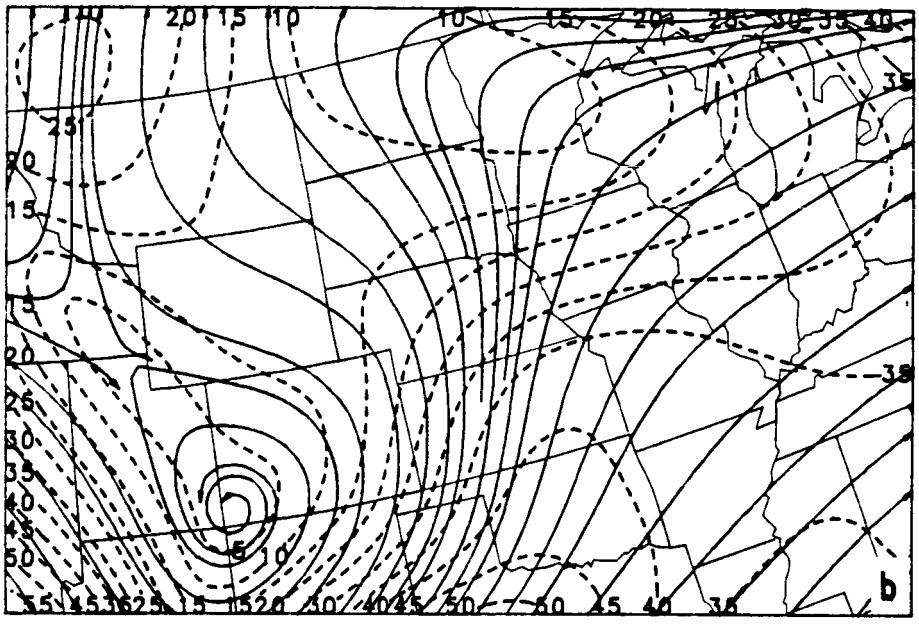

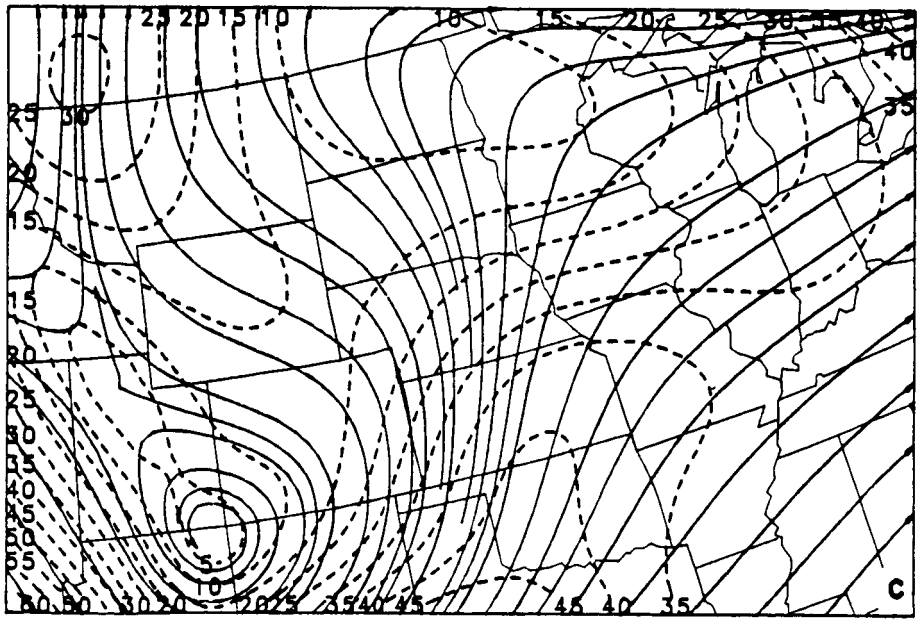

Fig. 10

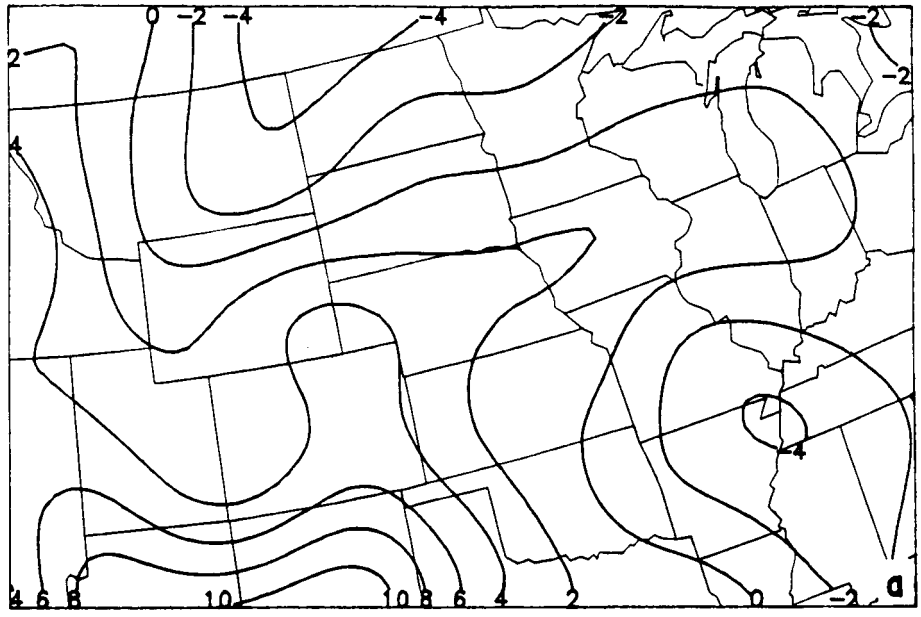

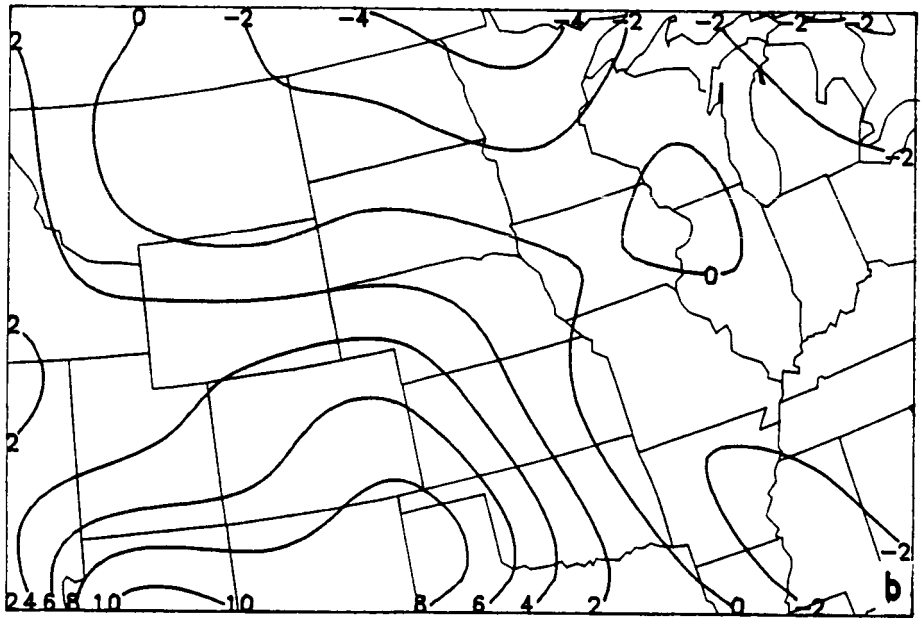

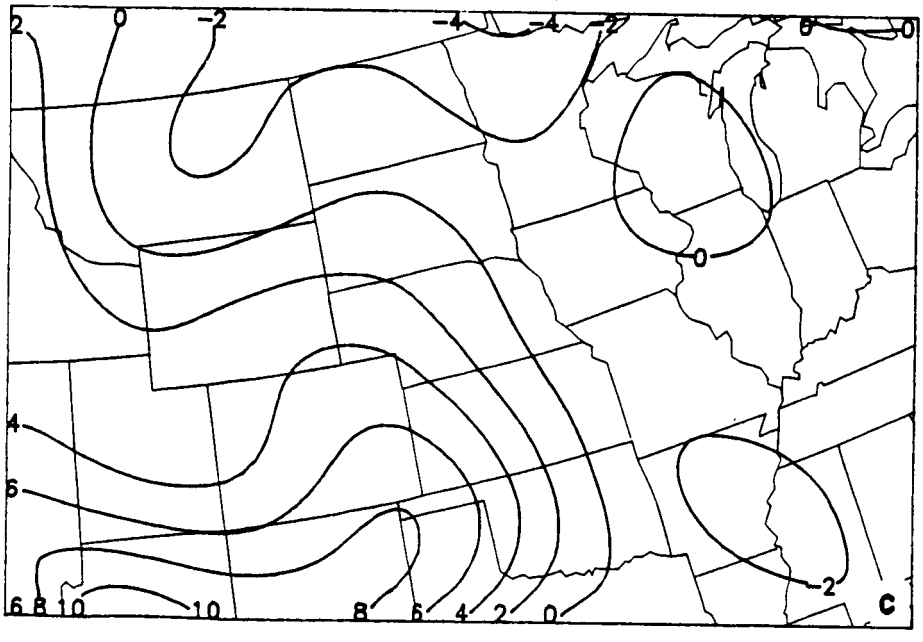

Fig. 11

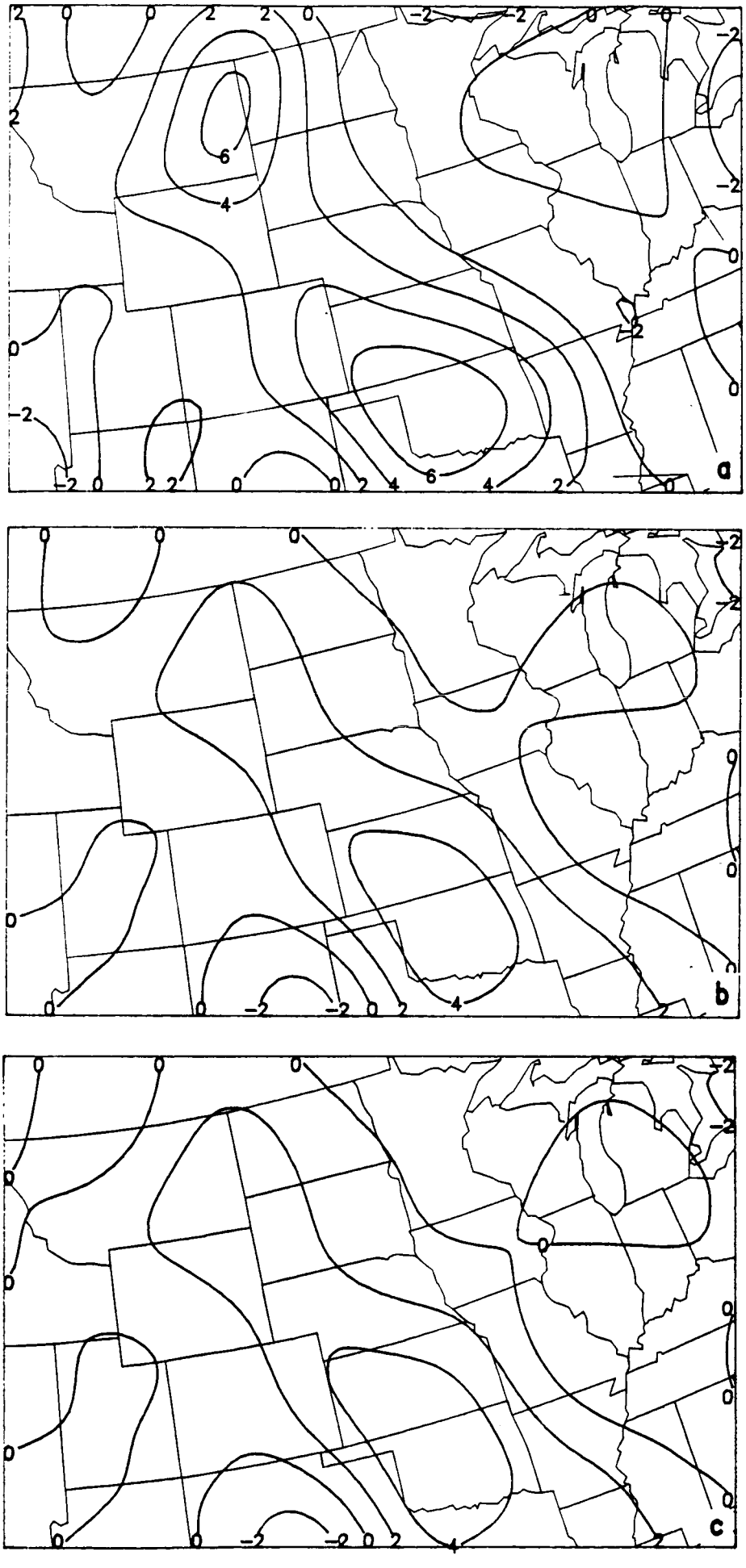

Fig. 12

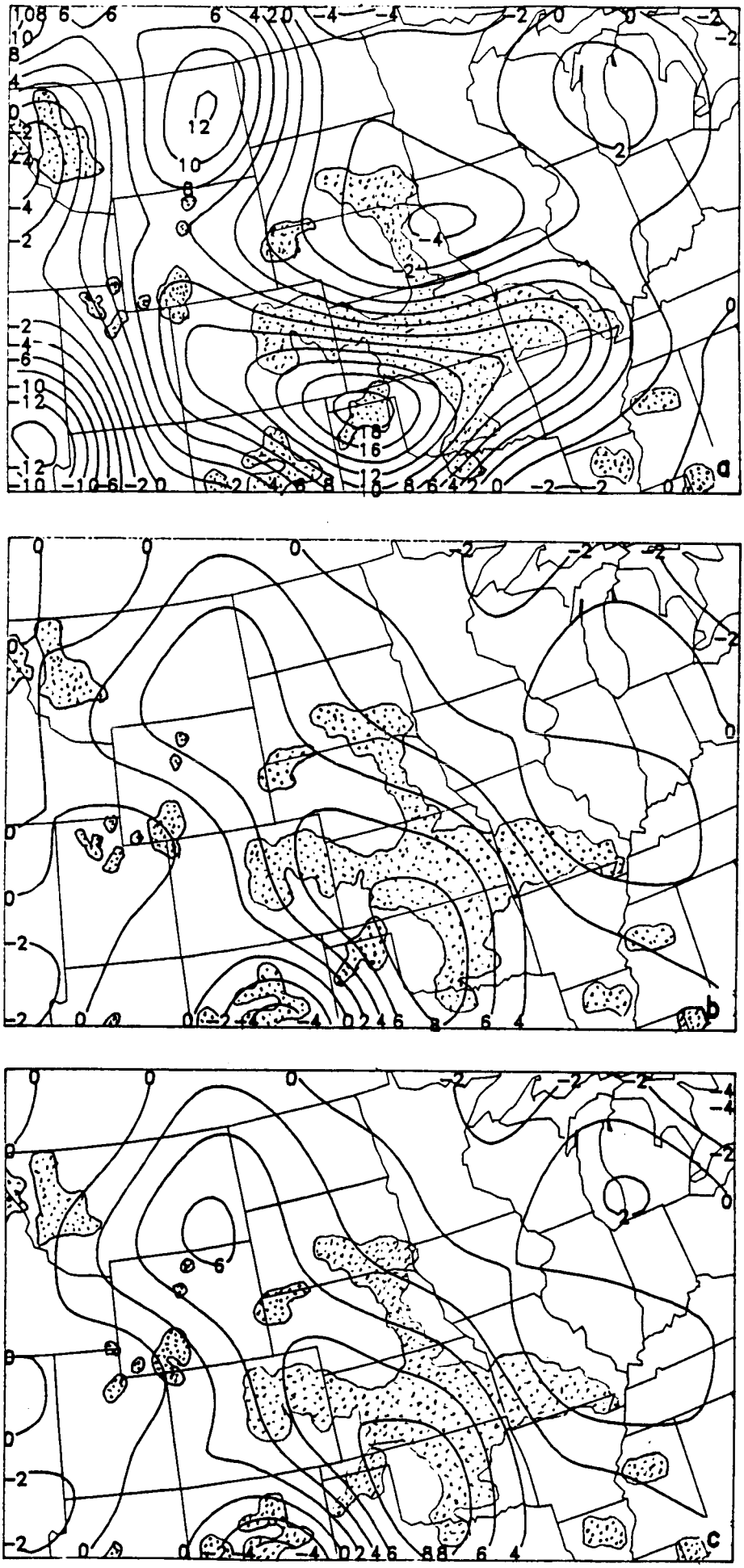

Fig. 13

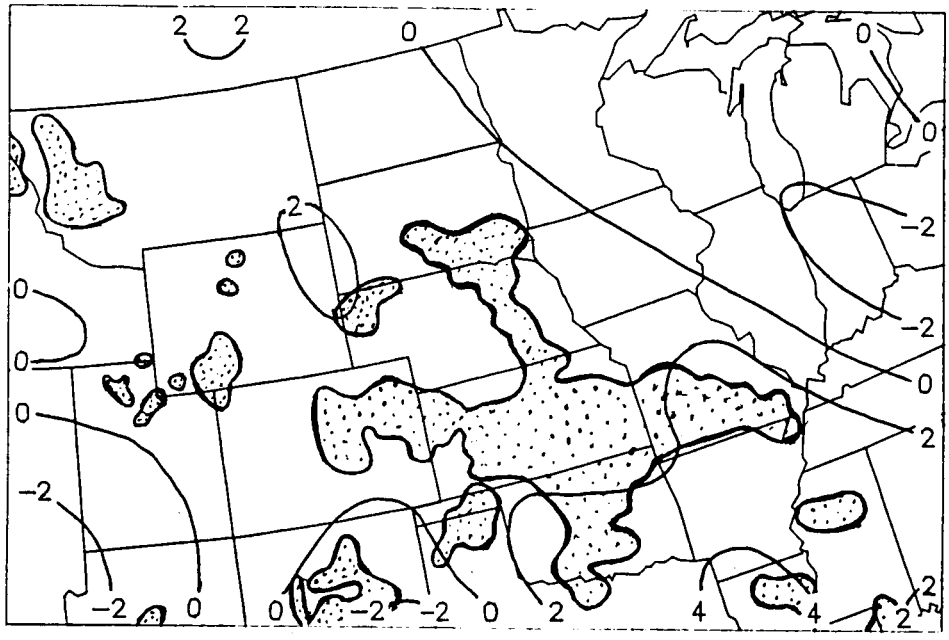

Fig. 14

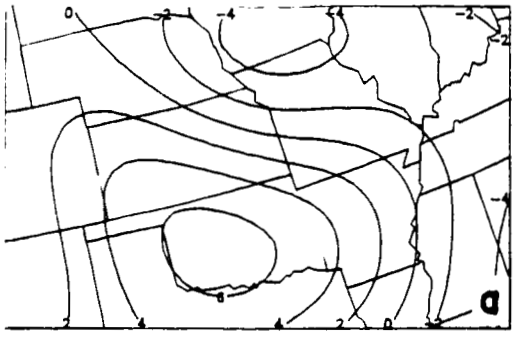

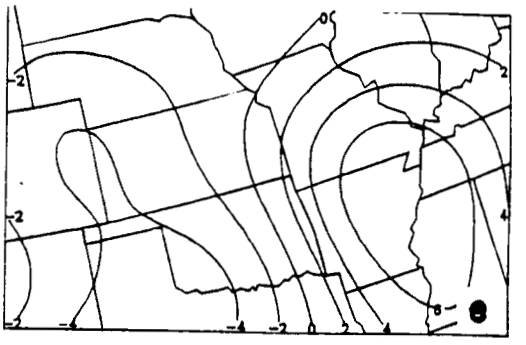

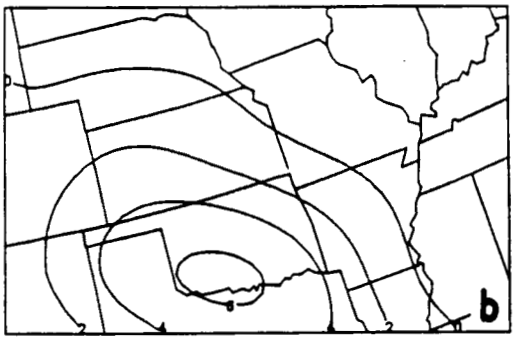

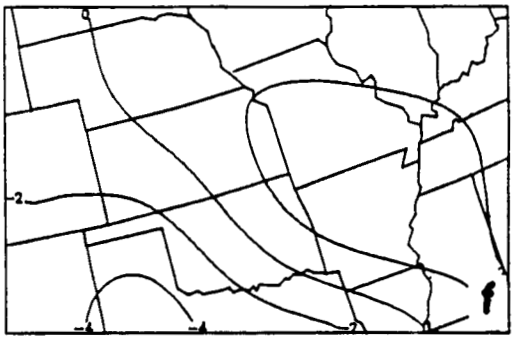

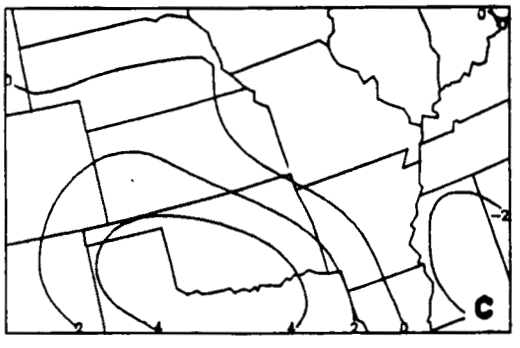

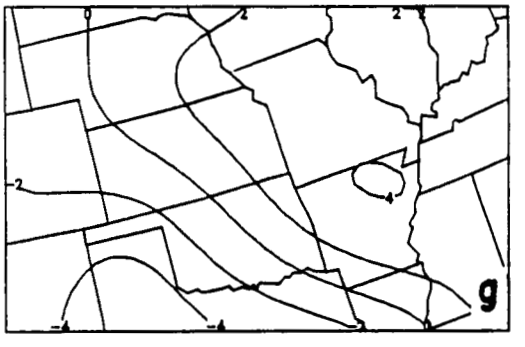

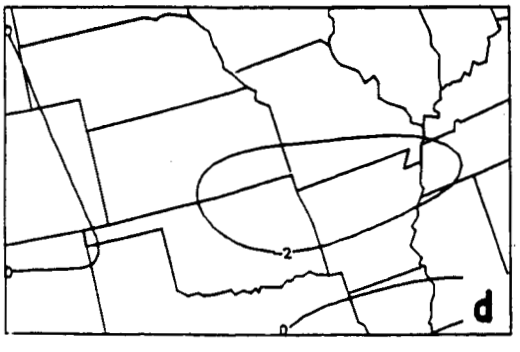

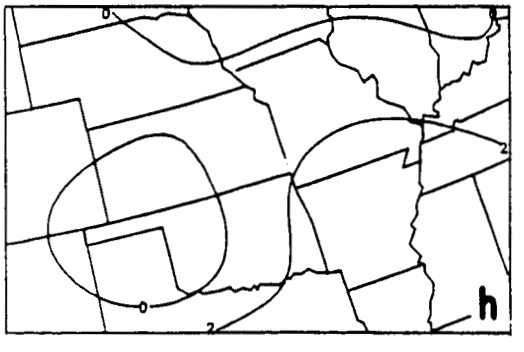

Fig. 15

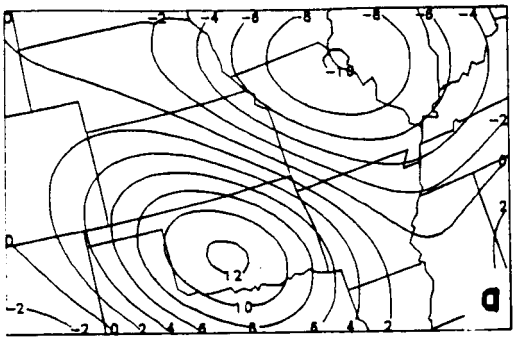

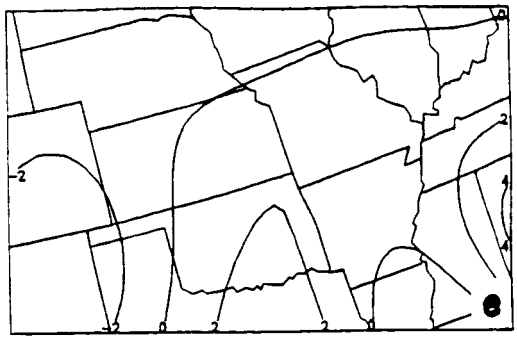

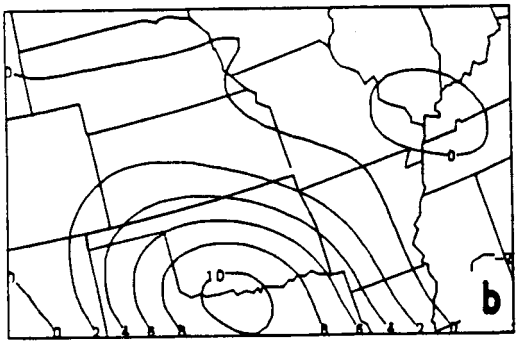

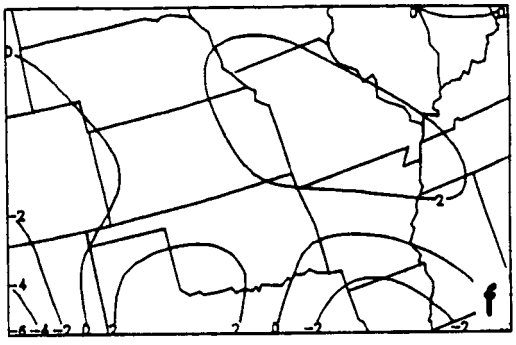

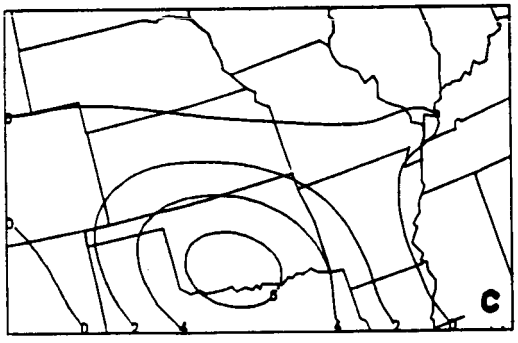

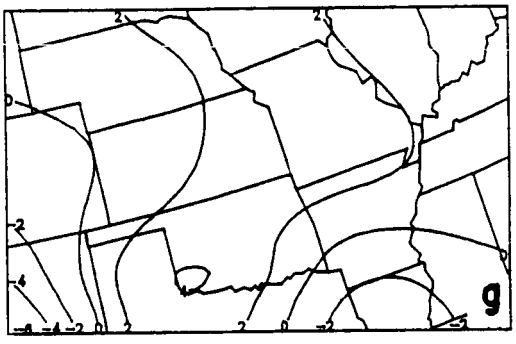

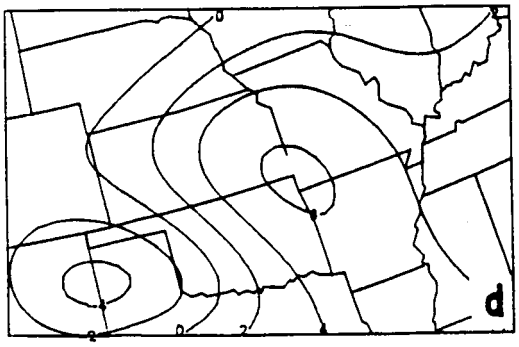

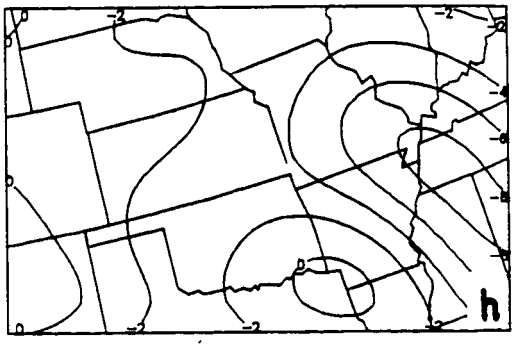

Fig. 16

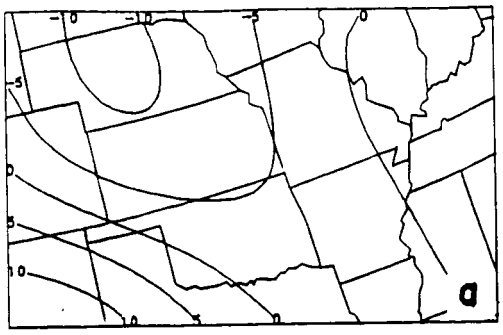

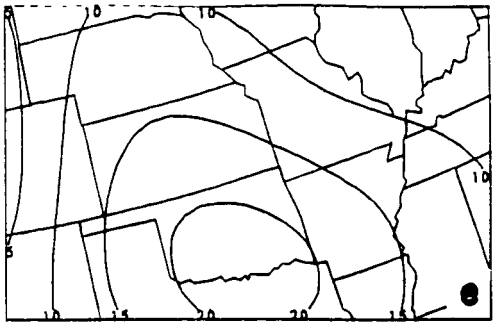

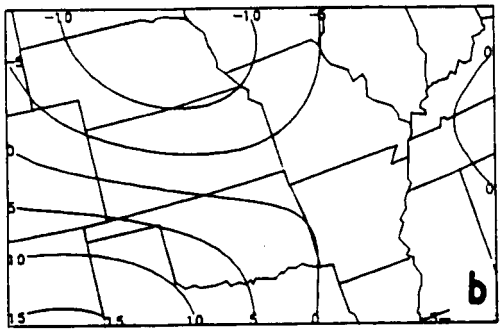

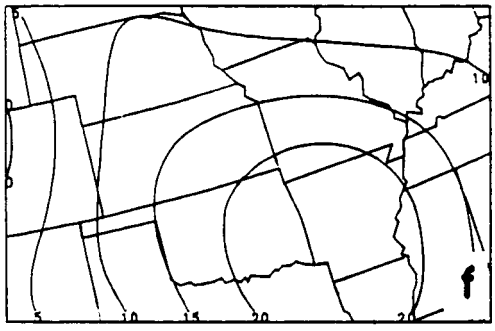

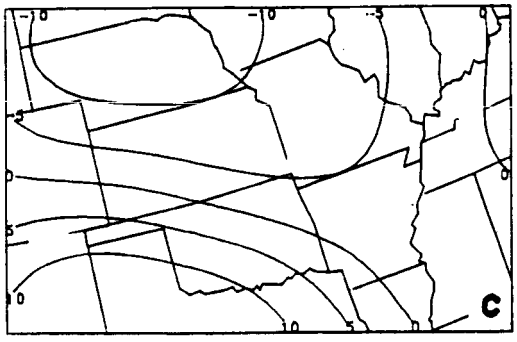

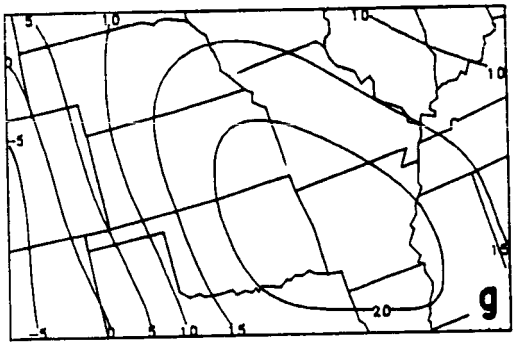

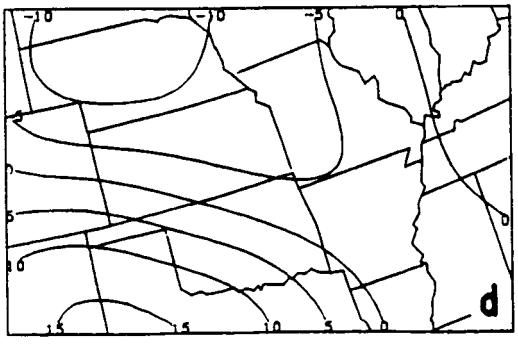

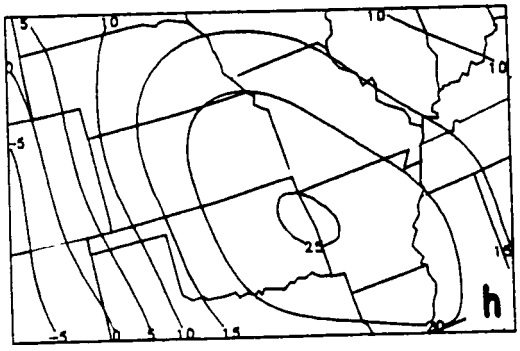

Fig 17

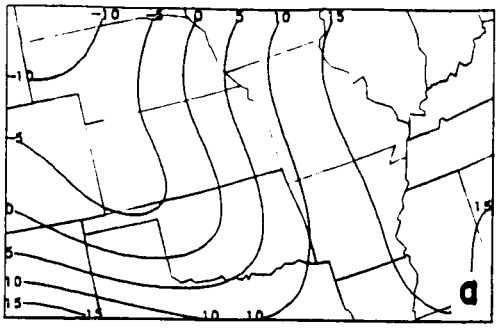

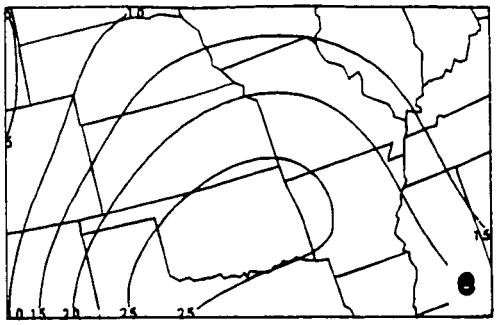

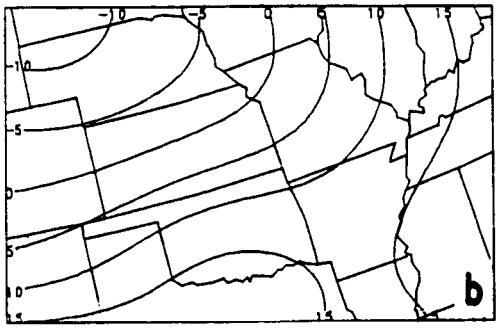

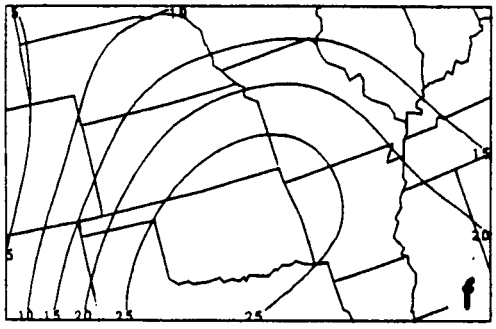

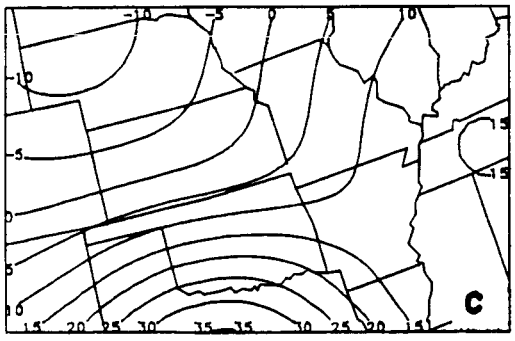

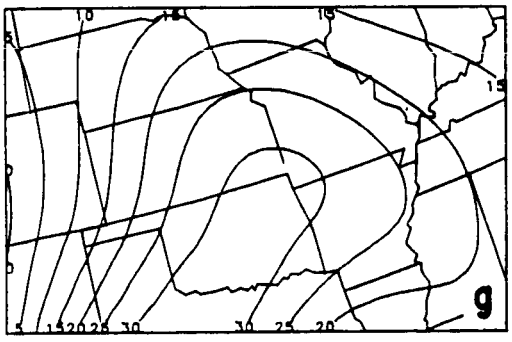

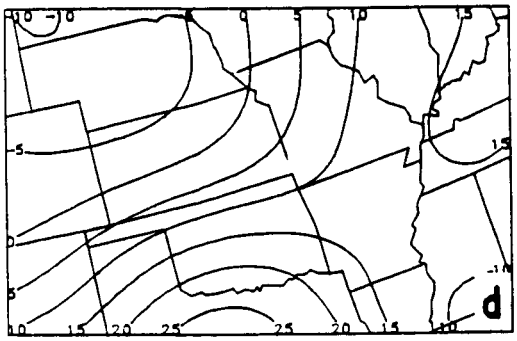

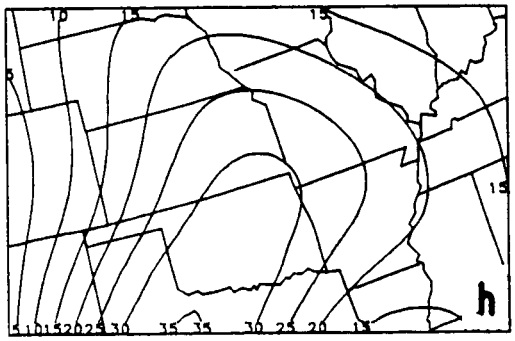

Fig 18